

## Original Article

**Cite this article:** Okay AI, Altiner D, Danelian T, Topuz G, Özcan E, and Kylander-Clark ARC (2022) Subduction-accretion complex with boninitic ophiolite slices and Triassic limestone seamounts: Ankara Mélange, central Anatolia. *Geological Magazine* **159**: 1699–1726. <https://doi.org/10.1017/S0016756822000504>

Received: 14 January 2022

Revised: 26 March 2022

Accepted: 4 May 2022

First published online: 10 June 2022


**Keywords:**

ophiolitic mélange; subduction; Turkey; Triassic; Jurassic; boninite; foraminifera

**Author for correspondence:** Aral I. Okay,

Email: [okay@itu.edu.tr](mailto:okay@itu.edu.tr)

# Subduction-accretion complex with boninitic ophiolite slices and Triassic limestone seamounts: Ankara Mélange, central Anatolia

Aral I Okay<sup>1,2</sup> , Demir Altiner<sup>3</sup>, Taniel Danelian<sup>4</sup>, Gültekin Topuz<sup>1</sup>, Ercan Özcan<sup>2</sup> and Andrew RC Kylander-Clark<sup>5</sup>

<sup>1</sup>Eurasia Institute of Earth Sciences, Istanbul Technical University, Maslak, Sariyer, Istanbul, Turkey; <sup>2</sup>Department of Geological Engineering, Istanbul Technical University, Faculty of Mines, Maslak, Sariyer, Istanbul, Turkey; <sup>3</sup>Department of Geological Engineering, Middle East Technical University, Ankara, Turkey; <sup>4</sup>Univ. Lille, CNRS, UMR 8198 – Evo-Eco-Paléo, F-59000 Lille, France and <sup>5</sup>Department of Earth Sciences, University of California, Santa Barbara, California, USA

**Abstract**

Ophiolitic mélanges in Anatolia represent Mesozoic subduction-accretion complexes, which are unusually poor in land-derived coarse-clastic rocks. A segment of the ophiolitic mélange in the Beynam region south of Ankara was studied. The ophiolitic mélange consists of three accretionary units (AUs), which are distinguished by lithology, structure, age and geochemistry. At the base there is a serpentinite mélange, which is overlain by a semi-intact Upper Jurassic ophiolite with boninite geochemistry. The topmost AU consists of ocean-island-like alkali basalts with seamount-derived Triassic shallow-marine limestones and Jurassic radiolarian cherts, which are stratigraphically overlain by Upper Cretaceous fore-arc turbidites. The base of the fore-arc sequence is palaeontologically and isotopically dated to the early to middle Campanian (c. 81 Ma). Detrital zircons from the fore-arc sequence indicate a Late Cretaceous (87–81 Ma) magmatic arc as a source. The formation of the subduction-accretion complex was a two-stage process. The first stage took place during the Late Jurassic – Early Cretaceous, when supra-subduction type oceanic crust was generated, and subduction accretion was intra-oceanic. In the second stage during the Late Cretaceous the subduction jumped inboard, creating an Andean-type convergent margin, and the Jurassic oceanic crust was incorporated in the subduction-accretion complex. The lack of land-derived sandstones in the ophiolitic mélange can be attributed to the intra-oceanic subduction and to the limestone deposition in the upper plate during the main phase of subduction accretion in the Late Jurassic – Early Cretaceous.

**1. Introduction**

Subduction-accretion complexes constitute a major part of the active continental margin, forming belts hundreds of kilometres wide and more than 1000 km long, as for example in the present-day Makran (e.g. McCall & Kidd, 1982; Burg, 2018). Old subduction-accretion complexes, such as the Jurassic–Palaeogene Franciscan Complex of the western US (e.g. Ernst, 2011; Wakabayashi, 2015; Raymond, 2018) or the Cretaceous to Miocene Shimanto belt in Japan (e.g. Taira *et al.* 1988), make up a significant part of the orogenic belts. They also provide important information on the ages of the former oceanic lithosphere, of oceanic seamounts and plateaus, and of subduction in the old convergent margins.

Subduction-accretion complexes consist of two contrasting rock associations: (a) tectonic slivers of the down-going oceanic crust, which constitute the ophiolitic part, and (b) clastic rocks derived from the erosion of the continental magmatic arc, which constitute the trench turbidites (e.g. Isozaki, 1997; Wakita & Metcalfe, 2005; Kusky *et al.* 2013). In large subduction-accretion complexes, such as the Franciscan, Shimanto or Makran, sandstones form the bulk. In contrast, sandstones are rare in the ophiolitic mélanges in Anatolia, which represent Mesozoic Tethyan subduction-accretion complexes (e.g. Okay *et al.* 1998, 2019; Parlak & Robertson, 2004; Plunder *et al.* 2013; Pandeli *et al.* 2018; Robertson *et al.* 2021). Here we describe a well-exposed segment of the ophiolitic mélange in the Beynam–Ankara region, depict its evolution and discuss the reason for the lack of the coarse-clastic component. In the Beynam area, the ophiolitic mélange is stratigraphically overlain by Upper Cretaceous fore-arc turbidites, which allows reconstruction of the geometry during the Late Cretaceous subduction-accretion.

The ophiolitic mélange in the Beynam–Ankara region consists of three distinct accretionary units (AUs) in the sense of Raymond *et al.* (2020), lithologically distinctive, mappable and fault-bounded rock bodies that were formed during subduction accretion and consist of lithologic or tectonostratigraphic units truncated at the AU margin by major faults.

© The Author(s), 2022. Published by Cambridge University Press. This is an Open Access article, distributed under the terms of the Creative Commons Attribution licence (<http://creativecommons.org/licenses/by/4.0/>), which permits unrestricted re-use, distribution and reproduction, provided the original article is properly cited.



## 2. Geological setting

Mesozoic subduction-accretion complexes, generally named as ophiolitic mélangé, crop out over large areas along the İzmir–Ankara suture, that marks the boundary between the Pontides and the Anatolide–Tauride Block (Fig. 1). They represent remnants of a Mesozoic Tethyan ocean, which separated Pontides in the north, from the Anatolide–Tauride Block and the Kırşehir Massif in the south (e.g. Şengör & Yılmaz, 1981; Robertson *et al.* 2009; Mueller *et al.* 2019; Okay *et al.* 2020a; van Hinsbergen *et al.* 2020). The ophiolitic mélangés in central Anatolia constitute part of the Ankara Mélangé, one of the earliest mélangés described (Bailey & McCallien, 1950, 1953). The Ankara Mélangé is made up of two distinct subduction-accretion complexes: the Karakaya Complex in the west and the ophiolitic mélangé in the east (Figs 1 and 2; e.g. Koçyiğit, 1991; Rojay, 2013). The Karakaya Complex forms a north–south-trending, 24 km wide belt in central Anatolia (Fig. 2). It consists of Permian and Carboniferous limestone blocks in a sheared Upper Triassic greywacke matrix (Upper Karakaya Complex) and a tectonically underlying sequence of metabasite, marble and phyllite (Lower Karakaya Complex). The Karakaya Complex is generally interpreted as a subduction-accretion unit, which was accreted to the southern margin of Laurasia during the Late Triassic (e.g. Robertson & Ustaömer, 2012; Okay & Nikishin, 2015). Subsequently the Karakaya Complex is unconformably overlain by Lower to Middle Jurassic sandstones and shales, which pass up into Upper Jurassic – Lower Cretaceous limestones, erosional remnants of which are preserved in a few places in the Ankara region (Figs 2 and 3; Bilgütay, 1960; Koçyiğit, 1989; Dönmez *et al.* 2008).

East of Ankara the Karakaya Complex is thrust eastwards over the ophiolitic mélangé (Fig. 2; e.g. Rojay, 2013). The ophiolitic mélangé consists of basalt, serpentinite, radiolarian chert and lesser amounts of pelagic shale and limestone. It forms a 13 km wide belt, and is thrust eastwards over the Upper Cretaceous turbidites, which are in turn thrust eastwards onto Palaeocene and Eocene clastic rocks (Fig. 2; Norman, 1972). Eocene sandstones and limestones also lie unconformably over the crystalline rocks of the Kırşehir Massif and constitute the oldest post-collisional marine sedimentary cover over the İzmir–Ankara suture (e.g. Gülyüz *et al.* 2013; Okay *et al.* 2020b).

The Kırşehir Massif consists of gneiss, marble and amphibolite with Late Cretaceous metamorphic ages (91–83 Ma) and dismembered ophiolites, which were intruded by Late Cretaceous granites to gabbros (85–65 Ma; Whitney & Hamilton, 2004; Lefebvre *et al.* 2011; van Hinsbergen *et al.* 2016). It was a continental terrane, with affinities to the Anatolide–Tauride Block, which underwent metamorphism under an obducted Cretaceous ophiolite followed by the development of a magmatic arc during the Late Cretaceous. The collision of the Kırşehir arc with the Pontides occurred in the late Maastrichtian – Palaeocene and produced the arc-shaped geometry of the central Pontides (Fig. 1; Kaymakçı *et al.* 2009; Meijers *et al.* 2010) and the present-day triangular shape of the Kırşehir Massif, which is a result of folding of the originally north–south-trending Kırşehir magmatic arc (Lefebvre *et al.* 2013).

## 3. Methods

The methods employed during this study include geological mapping, biostratigraphy, geochemistry and zircon U–Pb geochronology. Geological mapping was done on 1:25 000 scale topographic maps. The locations of samples and observation points are given in

UTM coordinates in Table S2 (in the Supplementary Material available online at <https://doi.org/10.1017/S0016756822000504>). Samples collected during geological mapping were studied for planktonic and benthic foraminifera and for radiolaria. Planktonic and benthic foraminifera and calpionellids from the Mesozoic rocks were identified in thin-sections based on Zaninetti (1976), Altuner & Zaninetti (1980), Zaninetti *et al.* (1982), Al-Shaibani *et al.* (1983), Altuner (1991), Altuner & Özkan (1991), Martini *et al.* (2004, 2009), Premoli Silva & Verga (2004) and Senowbari-Daryan & Link (2017). Larger benthic foraminifera (nummulitids, orthophragminids) from the Eocene sequence were studied both in thin-section and as loose individual foraminifera. The latter have been sectioned through the equatorial and axial planes for taxonomic studies.

Six samples of red radiolarian cherts were processed at the University of Lille with diluted hydrofluoric acid (HF 4 %) for at least three repetitive leachings, *c.* 24 hours each. Residues obtained from acid leaching were washed with the help of a 63 µm mesh sieve. Radiolarians were picked under a stereo-binocular microscope with an eyebrow, mounted on a thin brush stick. They were then mounted on SEM stubs and photographed with a ZEISS EVO scanning electron microscope.

Mineral separation for zircon dating was done in the Istanbul Technical University using classical techniques including crushing, sieving, magnetic and heavy liquid separation. The zircons were picked under a binocular microscope, mounted in epoxy and polished to nearly half-width of the grains. Internal structures of the mounted zircons were imaged by means of cathodoluminescence (CL) in the Hacettepe University (Ankara) by ZeissEvo-50SEM. The CL images of the analysed zircons are given in Figure S1 (in the Supplementary Material available online at <https://doi.org/10.1017/S0016756822000504>). Zircons were analysed using laser ablation – inductively coupled plasma – mass spectrometry (LA-ICP-MS) at the University of California, Santa Barbara. For details of the method employed, see Kylander-Clark *et al.* (2013) and Okay *et al.* (2020a). Long-term reproducibility in secondary reference materials is <2 % and, as such, should be used when comparing ages obtained within this analytical session to ages elsewhere. The U–Pb analytical data are given in Table 1 and Table S1 (in the Supplementary Material available online at <https://doi.org/10.1017/S0016756822000504>).

Whole-rock analyses were performed at Bureau Veritas Mineral Laboratories in Vancouver, Canada. A 1–5 kg sample was first processed in a steel jaw crusher, and an aliquot of *c.* 30 g was powdered in an agate rind-disc mill. Rock powders were then dried at 105 °C for *c.* 24 hours, and were sent for analysis. Accuracy is reported to be better than 2 % for major- and better than 10 % for trace-element analysis. For details of the analysis procedure see <https://commodities.bureauveritas.com/metals-minerals/exploration-and-mining/geoanalytical-services>.

Brief petrographic descriptions of samples analysed for geochemistry and/or for geochronology are given in the Supplementary Material (available online at <https://doi.org/10.1017/S0016756822000504>), along with their UTM locations and representative microphotos.

## 4. Geology of the Beynam area

The ophiolitic mélangé in the Beynam area south of Ankara was previously briefly described by Sarifakioğlu *et al.* (2017), and a 1:100 000 scale geological quadrangle map including the Beynam area was published by Akyürek *et al.* (1997). In the Beynam region the ophiolitic mélangé forms a sub-vertical tectonic sequence



**Fig. 1.** (Colour online) (a) Outcrops of the subduction-accretion complexes, ophiolites and magmatic arc rocks in western and central Turkey (modified from Okay *et al.* 2020a). (b) Tectonic map of the Eastern Mediterranean – Black Sea region (modified from Okay & Tüysüz, 1999).

unconformably overlain by the Upper Cretaceous fore-arc turbidites (Figs 4 and 5a). At present the unconformity surface dips steeply north at 70–80°. When the unconformity surface is restored to its original Late Cretaceous horizontal position, the underlying

ophiolitic melange provides a well-exposed 6 km thick vertical section of the subduction-accretion complex. The section consists of three well-defined fault-bounded tectonic slices, called accretionary units (AUs), which have thickness of a few kilometres and lengths of



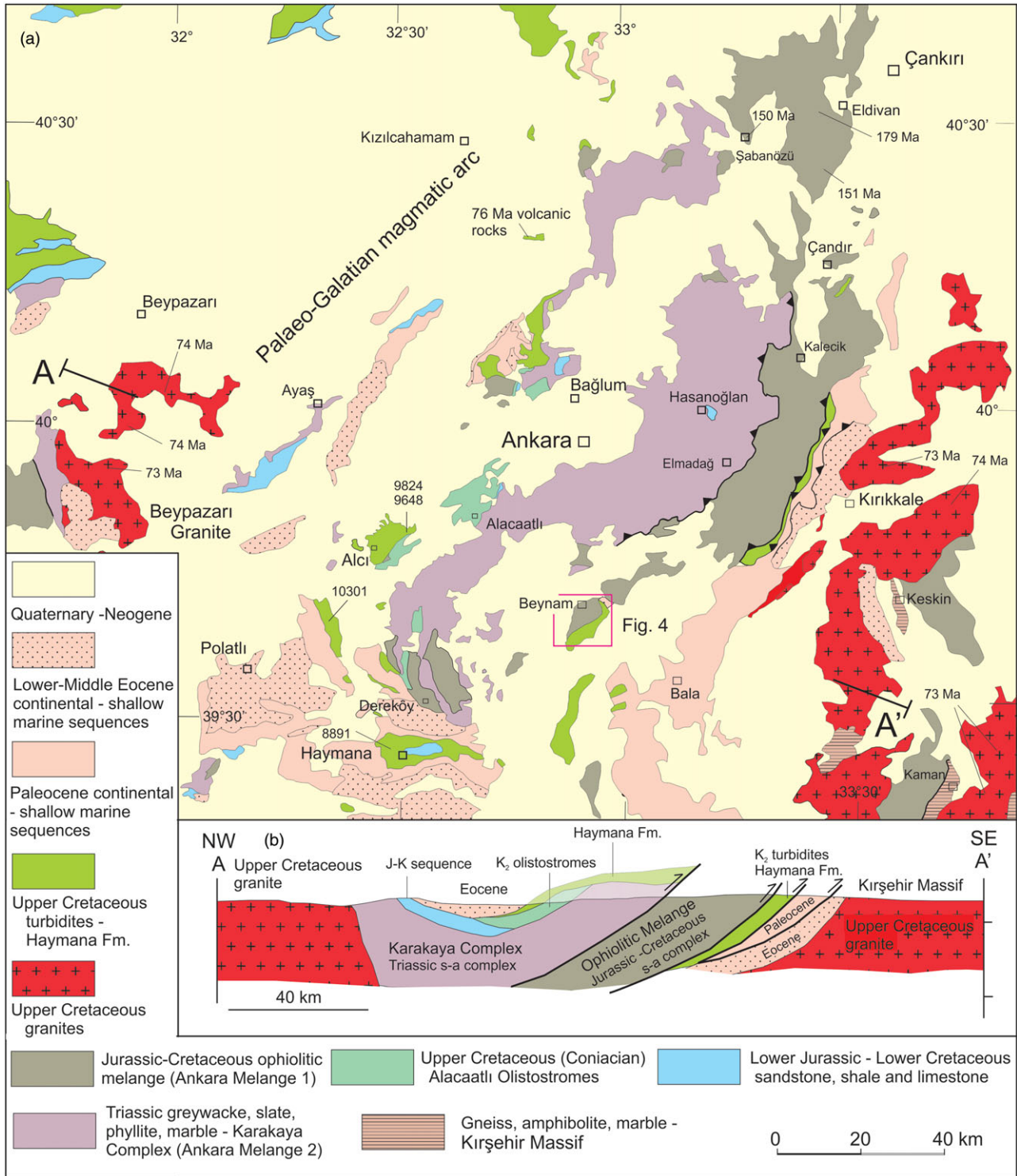


**Fig. 2.** (Colour online) (a) Geological map of the Ankara region modified from Turhan (2002) and Şenel (2002). The location of the study area is shown. (b) Schematic cross-section showing the relation between different tectono-stratigraphic units; s-a: subduction accretion, J-K: Jurassic-Cretaceous, K<sub>2</sub>: Upper Cretaceous. For the sources of the isotopic ages see the text.

over 8 km (Fig. 4). During the Late Cretaceous the tectonic stack consisted of the Kuyumcudağ AU at the base, overlain by Otlubel and Holos AUs. Below we describe the AUs from base upwards.

**4.1. Kuyumcudağ Accretionary Unit: serpentinite mélangé**

Kuyumcudağ AU consists of a serpentinite mélangé. It dips at c. 70° to the NW, has a minimum structural thickness of c. 1 km

(Figs 4 and 5a) and continues northwest under the Neogene sedimentary cover. It lies with a steep fault contact over the Otlubel AU.

About 70 % of the Kuyumcudağ AU consists of variably serpentinized, foliated or blocky harzburgites, and the rest consists of tectonic blocks of basalt, Jurassic red radiolarian chert and limestone (Fig. 5b, c). Foliation in the serpentinite dips steeply NW. Petrographically the basalt consists of plagioclase, augite and late

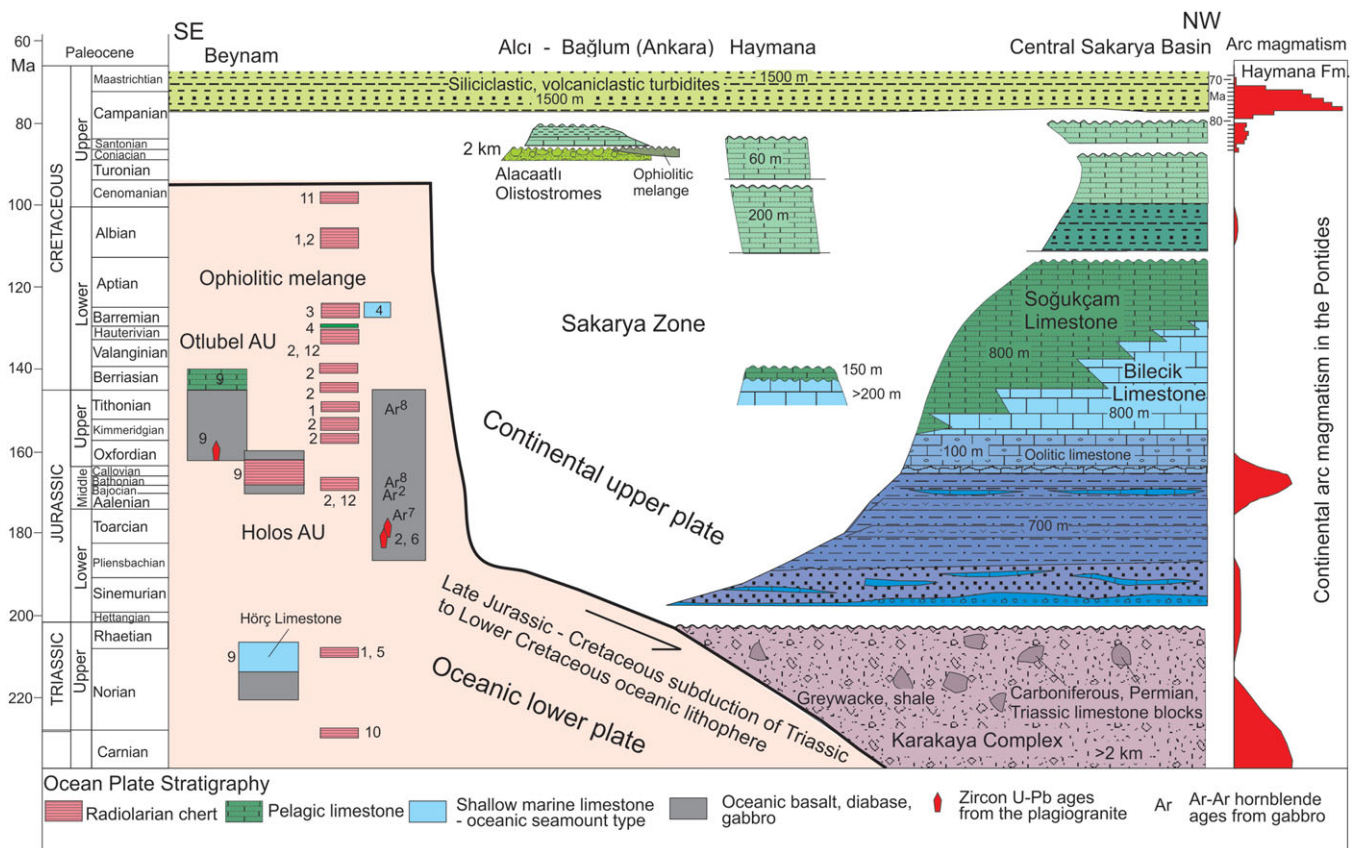


**Fig. 3.** (Colour online) Stratigraphic column showing the palaeontological and isotopic ages from the ophiolitic mélanges from western and central Anatolia, the stratigraphic sections of the Sakarya Zone, and periods of arc magmatism in the Pontides. The sources for the age data are: 1 – Bragin & Tekin (1996); 2 – Sarıfakıoğlu *et al.* (2017); 3 – Bortolotti *et al.* (2018); 4 – Rojay *et al.* (2004); 5 – Bortolotti *et al.* (2013); 6 – Dilek & Thy (2006); 7 – Çelik *et al.* (2011); 8 – Çelik *et al.* (2013); 9 – this study; 10 – Tekin *et al.* (2002); 11 – Gönçüoğlu *et al.* (2006); 12 – Özkan *et al.* (2020).

chlorite and calcite. Sarıfakıoğlu *et al.* (2017) report Middle to Late Jurassic radiolaria ages from four chert samples, which are shown on the geological map in Figure 4. The sizes of the blocks range from a few metres to *c.* 50 m. The blocks tend to be aligned and define a steeply dipping tectonic fabric (Fig. 5c).

#### 4.2. Otlubel Accretionary Unit: Late Jurassic oceanic crust with boninite chemistry

The sub-vertical Otlubel AU has a structural thickness of ~1.8 km. It consists mainly of basalt and diabase with lesser amounts of gabbro, plagiogranite, conglomerate and pelagic limestone. The Otlubel AU shows a stratigraphy with thin lenses of gabbro in the north passing up to a thick layer of Jurassic basalt and diabase with small veins and patches of plagiogranite, overlain by debris flow conglomerates intercalated with basaltic flows, which pass up into Lower Cretaceous pelagic limestones (Figs 4 and 5a).

The gabbro occurs as thin (<30 m) lenses on the northern margin of the Otlubel AU. It consists of plagioclase (An<sub>62</sub>) and hornblende with minor pyroxene, quartz and late epidote. Basalt and diabase are the dominant rock types in the Otlubel AU and make up more than 80 % of the bulk. They occur as lava flows showing agglomerate and pillow lava structures. Locally diabase is cut by isolated basaltic dykes, which, however, make up a few per cent of the Otlubel AU. The primary igneous mineral assemblage in the diabase and basalt is plagioclase and hornblende with minor

augite and opaque minerals (cf. Supplementary Material available online at <https://doi.org/10.1017/S0016756822000504>); augite is preserved only in 4 out of 20 samples petrographically examined. Secondary minerals include chlorite, actinolite, epidote and calcite.

The diabase is locally cut by plagiogranite veins, which form an irregular network and are generally tens of centimetres wide (Fig. 6a). The plagiogranite consists mainly of quartz and plagioclase with minor hornblende and opaque; secondary minerals include actinolite, chlorite and epidote. It makes up less than 0.1 % of the Otlubel AU. Out of three plagiogranite samples processed, only one (sample 12526) yielded four zircons, all of which contained appreciable common Pb (Table 1). Though a 204-based common-Pb correction proves challenging (low 204 counts, Hg interference etc.), it nevertheless yields equivalent Late Jurassic (Oxfordian) dates of  $161.2 \pm 3.2$  Ma for two of the four grains. The other two zircons yield Late Carboniferous ages. Late Jurassic ( $150 \pm 4$  Ma) Ar–Ar hornblende ages from ophiolitic gabbros are also reported by Çelik *et al.* (2013) from further north in the Eldivan region (Fig. 2). Plagiogranites from the Eldivan region produced Early Jurassic (*c.* 180 Ma) zircon U–Pb ages (Dilek & Thy, 2006; Sarıfakıoğlu *et al.* 2017). Early Jurassic (174–183 Ma) plagiogranite and diabase bodies are also described from the ophiolitic mélanges and from the largely intact ophiolite bodies along the İzmir–Ankara suture (Robertson *et al.* 2013; Topuz *et al.* 2013; Uysal *et al.* 2013; Sarıfakıoğlu *et al.* 2017; Balcı & Sayit, 2020; Okay *et al.* 2020a).

**Table 1.** U–Pb data from zircons from a plagiogranite vein in the Otlubel AU, Ankara mélange (sample 12526)

Grains	U ppm	Th ppm	No common-Pb correction					204-corrected data								
			$^{238}\text{U}/^{206}\text{Pb}$	$^{207}\text{Pb}/^{206}\text{Pb}$	$^{208}\text{Pb}/^{232}\text{Th}$	207-corr. age	Concordance	$c. \text{ }^{206}\text{Pb}/^{204}\text{Pb}$	$^{238}\text{U}/^{206}\text{Pb}$	$^{207}\text{Pb}/^{206}\text{Pb}$	$\rho$					
1	1312	1423	39.73	0.91	0.058	0.002	0.0082	0.0003	158	0.86	1921	40.12	1.28	0.050	0.002	-0.44
2	277	376	35.86	0.84	0.108	0.008	0.0108	0.0005	164	0.50	256	38.64	1.25	0.051	0.008	-0.58
3	317	174	19.08	0.48	0.075	0.006	0.0178	0.0014	320	0.75	515	19.78	0.67	0.046	0.006	-0.15
4	210	92	19.44	0.44	0.105	0.003	0.0317	0.0012	302	0.57	306	20.67	0.66	0.057	0.004	0.75

The basalt and diabase are overlain by conglomerates with clasts of pelagic limestone and basalt in a volcanogenic argillaceous matrix (Fig. 6b). Although the actual contact is not well exposed, the absence of serpentinite slivers or foliation along the contact suggests that it is stratigraphic. The conglomerate beds are up to 15 m thick and are separated by basaltic flows (Fig. 6c). Poor sorting and angular clasts indicate that the conglomerates represent debris flows. The conglomerates are overlain by pelagic limestones, which crop out as a continuous 150 m thick horizon along the southern margin of the Otlubel AU (Figs 4 and 6d). The limestones are medium-bedded, light-grey, beige, radiolaria-bearing micrites with thin shale interbeds. Most limestone samples contain just calcified radiolaria tests; however, two samples comprise *Calpionella alpina*, *C. grandalpina*, *C. elliptica*, *Tintinnopsella carpathica*, *Crassicollaria parvula* and *Remaniella ferasini* (Fig. 7, photos 44–62) besides abundant radiolaria, which indicate an earliest Cretaceous (Berriasian) age. Sarıfakıoğlu *et al.* (2017) also report Early Cretaceous ages from the limestone horizon, including an Aptian–Albian radiolaria age. The age of the limestone is compatible with the Late Jurassic age of the underlying oceanic crust. The Lower Cretaceous limestones are tectonically underlain by a continuous serpentinite slice, 20 m to 300 m in thickness, which dips at high angles to the north (70–80°) and marks the boundary between the Otlubel and Holos AUs (Figs 4 and 6d). North of the village of Karaali the serpentinite slice merges to a larger area of serpentinite, locally with blocks of basalt and chert (Fig. 4).

#### 4.3. Holos Accretionary Unit: Triassic oceanic seamounts and Jurassic cherts

The Holos AU forms a sub-vertical tectonic slice between the Otlubel AU and the fore-arc turbidites, the Haymana Formation (Figs 4 and 5a). The Holos AU has a thickness of 2.1 km, and is made up predominantly of basalt (>65 %) with lesser amounts of Jurassic radiolarian chert, Triassic limestone and serpentinite. It differs from the Otlubel AU by the lack of any recognizable stratigraphy and by the presence of Triassic limestones, radiolarian cherts and serpentinite. Basalts in the Holos AU occur both as porphyritic pillow basalt with large white plagioclase phenocrysts set on a matrix of pinkish Ti-augite, plagioclase and opaque (Fig. 8f) and aphyric alkali basalts with a similar mineral assemblage. Some of the basalt samples contain analcime or kaersutite, attesting to their strongly alkaline character (cf. Supplementary Material available online at <https://doi.org/10.1017/S0016756822000504>). Kaersutite forms phenocrysts, up to 5 mm long, in a matrix of feldspar and opaque. Analcime occurs as idioblastic microphe-nocrysts in a matrix of augite, feldspar and opaque. Analcime was described previously from the basalts of the ophiolitic mélange in the Ankara Kalecik region (Çapan & Buket, 1975) and has been shown to be secondary after leucite (Varol, 2013). All the basalts show alteration involving formation of chlorite, calcite and epidote; the amygdales in the basalts are commonly filled by calcite. Serpentinite makes up less than 5 % of the Holos AU, occurs as steeply dipping narrow slivers, a few to tens of metres wide and up to a few hundred metres long, and marks tectonic contacts.

##### 4.3.1. Shallow marine Triassic limestones

A characteristic feature of the Holos AU is the presence of shallow marine Upper Triassic limestone blocks embedded in a volcanoclastic matrix (Fig. 8). This Hörç Limestone makes up *c.* 10 % of the Holos AU. Akyürek *et al.* (1997) have mapped these limestones



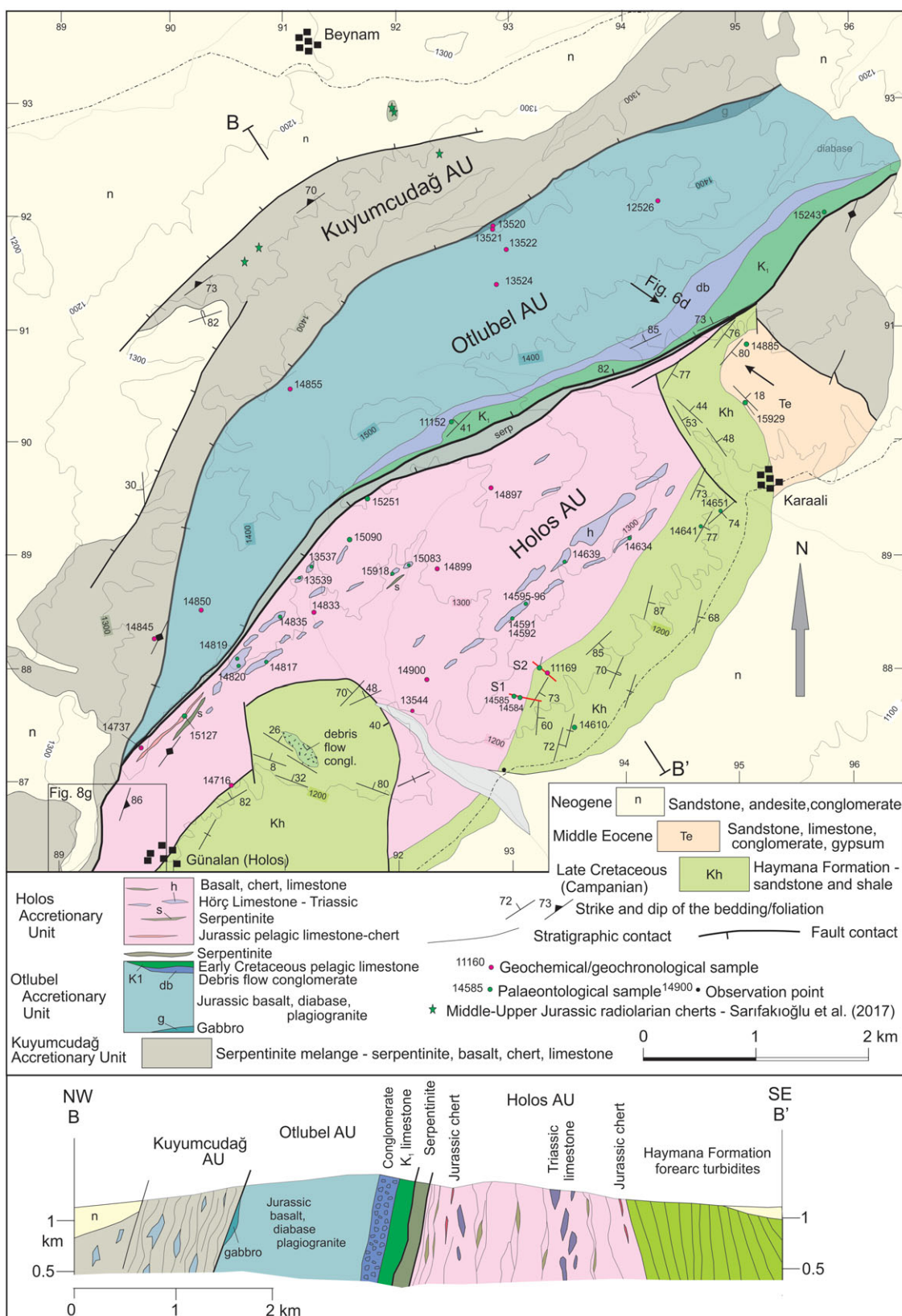


**Fig. 4.** (Colour online) Geological map and cross-section of the Beynam area (based on our mapping, Akyürek *et al.* 1997 and Sarıfakıoğlu *et al.* 2017). K<sub>1</sub>: Lower Cretaceous. For location see Figure 2.





**Fig. 5.** (Colour online) (a) Google Earth image of the Beynam area showing the well-exposed tectonic units and the Haymana Formation. Compare the image with the geological map in Figure 4. Note the steep tectonic fabric and the continuous Lower Cretaceous (K1) limestone horizon in the Otlubel AU. (b, c) Serpentinite mélangé of the Kuyumcudag AU with limestone, basalt and Jurassic radiolarian chert blocks in serpentinite. Notice the steeply dipping tectonic fabric, especially in (c).

as Lower Jurassic; Sarıfakioğlu *et al.* (2017) mentions the presence of Triassic limestone blocks in the Beynam area without giving any details. The Hôrç Limestone is white, pale-grey, massive and contains corals, algae, bivalves, belemnites and gastropods (Fig. 8f). There are also very rare pink, micritic limestone blocks of probable Late Triassic age with thin-shelled bivalves and ammonites, which may represent forereef facies. The size of the limestone clasts ranges from a few mm to 50 m (Fig. 8). They occur in debris flows locally with blocks of basalt (Fig. 8d). The debris flow conglomerates form two distinct horizons, which can be followed for more than 2 km along strike (Fig. 4). Large blocks are worked in

quarries, which allow three-dimensional observation of the blocks (Fig. 8b, c). More than 15 blocks were sampled for palaeontological study. They contain an Upper Triassic (upper Norian – Rhaetian) foraminiferal fauna including *Galeanella laticarinata*, *Galeanella? minuta*, *Siculocosta floriformis?*, *Miliolipora cuvillieri*, *Orthotrinaracia* sp., *Decapoolina schaeferae*, *Ophthalmidium leischneri*, *O. maximum*, *Triadodiscus eomesozoicus*, *Aulotortus communis*, *A. tumidus*, *A. planidiscoides*, *A. ex gr. sinuosus*, *Parvalamella praegaschei*, *P. friedli*, *Triasina hantkeni*, *Auloconus permodiscoides*, *Trocholina ultraspirata*, *Semiinvoluta* sp., *Foliotortus spinosus*, *Duotaxis birmanica*, *D. metula*, ‘*Tetrataxis*’ *humilis*, ‘*Tetrataxis*’



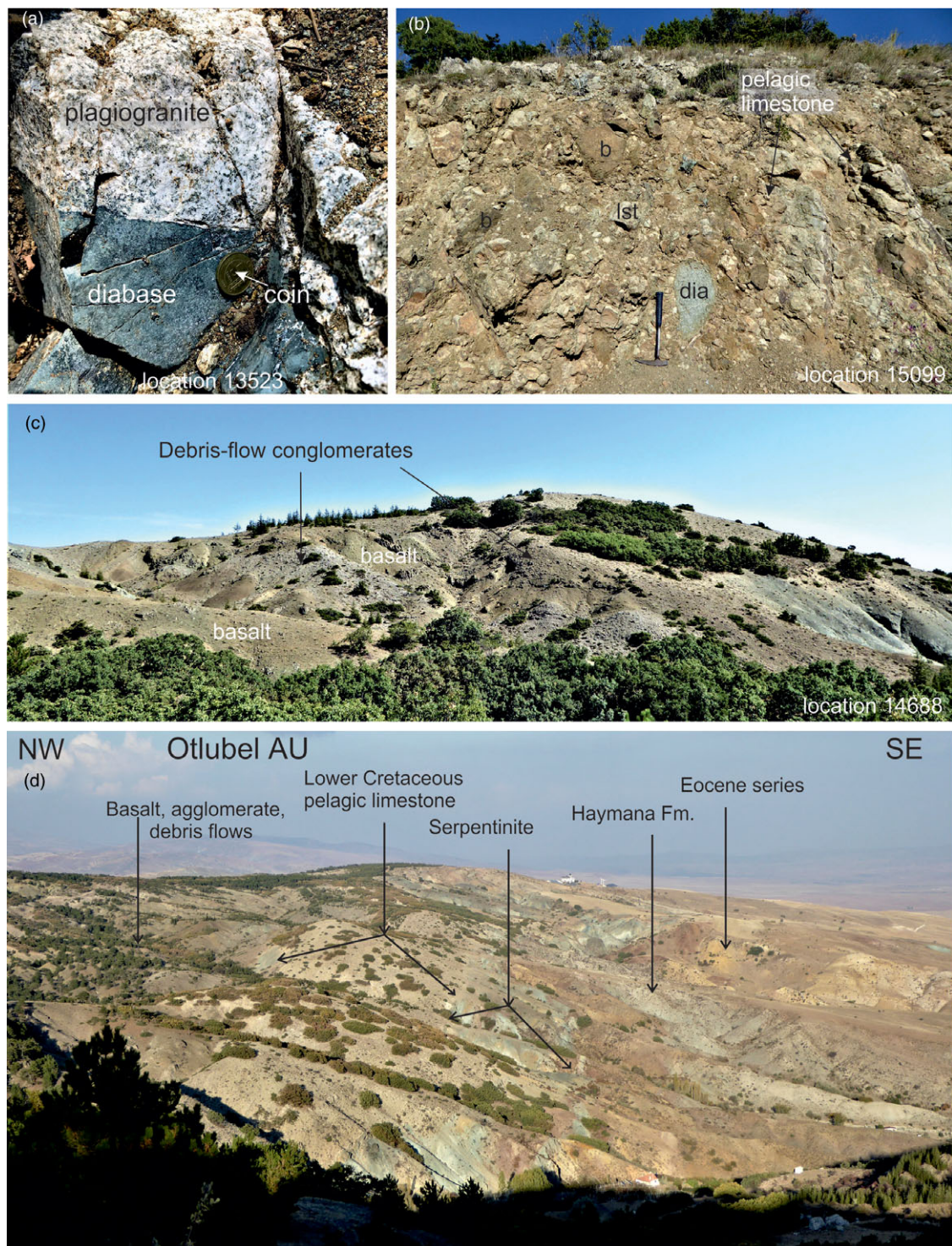


**Fig. 6.** (Colour online) Photographs of the Otlubel AU. (a) Diabase cut by Jurassic plagiogranite. (b) Debris flow conglomerate with poorly sorted clasts of basalt (b), diabase (dia) and pelagic limestone (lst). (c) Intercalation of basalt and conglomerate horizons. (d) Panoramic view of the southern contact of the Otlubel AU with the Lower Cretaceous pelagic limestone bounded by the serpentinite sliver. For location of the photograph see Figure 4.

*inflata*, *Trochammina jaunensis*, *Reophax tauricus*, *Gandinella falsofriedli*, *Glomospirella amplificata*, *Endoteba controversa*, *Dentalina vadaszi*, *Austrocolomia canaliculata*, *Polarisella* spp., *Globochaete* sp., *Thaumatoporella parvovesiculifera*, *Tubiphytes obscurus* and *Baccanella floriformis* (Fig. 7, photos 1–42 and Fig. 9).

#### 4.3.2. Jurassic radiolarian chert and pelagic limestone

Thinly bedded red radiolarian cherts occur as 5–20 m thick discontinuous horizons interbedded with red pelagic limestone and basalt. The radiolarian cherts occur throughout the Holos AU, and Jurassic radiolarian ages are determined from both its NW and SE margins. Red pelagic limestones did not produce any





**Fig. 7.** Microphotographs of the foraminifera (1–43, Upper Norian to Rhaetian blocks of the Hörz Limestone), calcionellids (44–53), planktonic foraminifera (54–68, basal part of the Haymana Formation) and other foraminifera and incertae sedis (69–71, from pebbles in the conglomeratic levels of the Haymana Formation). 1–3. *Duotaxis birmanica* Zaninetti and Brönnimann. 4–7, 8? *Duotaxis metula* Kristan. 9–10. *Tetrataxis humilis* Kristan. 11. *Tetrataxis inflata* Kristan. 12–15. *Trochammina* spp. 16–17, 18? *Trochammina jaunensis* Brönnimann and Page. 18–21. *Reophax tauricus* Zaninetti, Altiner, Dağer and Ducret. 22. *Glomospirella amplificata* Kristan-Tollmann. 23–25, 26?, 27. ? *Gandinella falsofriedli* (Salaj, Borza and Samuel). 28. *Pilamina?* sp. 29, 30?, 31. *Endoteba* sp. 32–33. *Endotriada* sp. 34. *Endoteba controversa* Vachard and Razgallah. 35. *Austrocolomia canaliculata* Oberhauser. 36–39, 41. *Polarisella* spp. 40. *Nodosarid* foraminifera. 42. *Dentalina vadaszi* Oberhauser. 43. *Textularia?* sp. 44. *Tintinnopsella carpathica* (Murgeanu and Filipescu). 45–47. *Calpionella alpina* Lorenz. 48. *Calpionella grandalpina* Nagy. 49–50. *Calpionella elliptica* Cadisch. 51. *Remaniella ferasini* (Catalano). 52–53. *Crassicollaria parvula* Remane. 54–55. *Globotruncana elevata* (Brotzen). 56. *Contusotruncana fornicata* (Plummer) or *Contusotruncana patelliformis* (Gandolfi). 57–58. *Globotruncana linneiana* (d'Orbigny). 59–60. *Globotruncana lapparenti* Brotzen. 61. *Globotruncana arca* (Cushman). 62–63. *Globotruncana bulloides* Vogler. 64. *Planoheterohelix globulosa* (Ehrenberg). 65. *Muricohedbergella monmouthensis* (Olsson). 66–67. *Muricohedbergella* spp. 68. *Macroglobigerinelloides bollii* (Pessagno) or *Macroglobigerinelloides prairiehillensis* (Pessagno). 69. *Charentia* sp. 70. *Mohlerina basilensis* (Mohler). 71–72. *Crescentiella morronensis* (Crescenti). 1–3, 7–8, 22, 26, 34, 36–37, 39: sample 14639; 4, 10, 15, 40: sample 13537; 5–16: sample 13539; 6, 21: sample 14820; 9, 14, 28, 38: sample 14817; 11, 19–20, 27: sample 14591; 12, 41: sample 14596; 13: sample 15083; 17–18, 23–25, 29–33: sample 14835; 35: sample 14592; 42: sample 14634; 44–45, 49–53: sample 11152; 46–48: sample 15243; 54, 60–62, 68: sample 14580; 55, 57, 59, 64, 66: sample 14581; 56, 63, 65: sample 14651; 58: sample 14610; 67: sample 14641; 69, 71: sample 14607; 70–72: sample 14616.



age diagnostic fossils, whereas several samples of radiolarian cherts contain a moderately well-preserved radiolarian fauna (Fig. 10) of Middle to Late Jurassic (Bathonian – Oxfordian) age. More particularly, sample 14584 yielded an age diagnostic species, *Kilinora* (?) *oblongula* (Fig. 10i), known to occur only in Unitary Association Zones (UAZ) 6–8 of the biozonation of Baumgartner *et al.* (1995); therefore sample 14584 may be correlated with the middle Bathonian to early Oxfordian time interval. The same age is deduced for sample 15127, as the co-occurrence of species *Archaeohagiastrum munitum* and *Paronaella mulleri* (Fig. 10m and n) allows its correlation with UAZ 6–8 of the biozonation of Baumgartner *et al.* (1995). Finally, sample 14585 may be assigned with certainty to the latest Bajocian/early Bathonian to late Oxfordian/early Kimmeridgian interval based on the presence of species *Palinandromeda podbielensis*, which is known from UAZ 5–9 of Baumgartner *et al.* (1995). Furthermore, the presence of a poorly preserved specimen, which has been tentatively identified as *Guexella nudata*, suggests that the age of this sample may possibly be restricted to the latest Bajocian/early Bathonian to early Oxfordian interval (UAZ 5–8).

### 5. Structure of the accretionary units

The ophiolitic mélange in the Beynam area does not show any regional metamorphism, and foliation is locally developed along shear zones and close to the contacts of the AUs, and is invariably steeply dipping (Fig. 8g). The steep fabric of the ophiolitic mélange is especially well marked in the Kuyumcudağ and Holos AUs. In the Kuyumcudağ AU, intense shearing is defined by sub-vertical foliation in the serpentinite; the blocks in the serpentinite also show a steep alignment. Shear zones are much rarer in the Otlubel AU (<3%), which appears to have largely preserved the oceanic crustal stratigraphy.

The Holos AU has a fabric characterized by the alignment of debris flow conglomerates, pelagic limestone, chert and serpentinite bodies (Figs 4, 5 and 8g). The repetition of the Triassic debris flow horizons and Jurassic cherts and limestones within the Holos AU (Fig. 4) indicates that it consists of an imbricated thrust stack. However, in the absence of a few metres thick serpentinite slivers, individual faults in the Holos AU are difficult to map. The thrust imbrication must have occurred during the subduction before the deposition of the Upper Cretaceous fore-arc turbidites. Shear zones, as opposed to faults, are rare in the Holos AU (<10% of the bulk, Fig. 8) and occur mainly close to its NW contact.

### 6. Geochemistry of the magmatic rocks in the ophiolitic mélange

Over 40 magmatic rock samples from the Beynam area were petrographically studied. The samples show low-temperature (subgreenschist facies) alteration involving formation of chlorite, calcite, epidote and pumpellyite. Among least altered samples fourteen were analysed for major and trace elements: six from Holos AU, seven from Otlubel AU and one from Kuyumcudağ AU. The locations of the samples are shown on the geological map in Figure 4, and the geochemical data are given in Table 2. Loss-on-ignition values range from 1.80 to 9.40 wt %, indicating the variably altered nature of the samples. The analysed samples are mostly basalt, andesite and diabase, with one gabbro and one plagiogranite.

The geochemical data reveal distinct differences in the geochemistry of the magmatic rocks from the Holos and Otlubel

AUs. All the mafic rocks from the Holos AU are alkaline (Fig. 11a, b), as also shown by the presence of analcime, kaersutite and T-augite in the mineral assemblage of some samples. On a volatile-free basis, the mafic rocks in the Holos AU have lower SiO<sub>2</sub> (46–54 wt %) and MgO (2.9–7.5 %) and higher Al<sub>2</sub>O<sub>3</sub> (13.7–21.2 %) and TiO<sub>2</sub> (1.0–3.6 %) than those from the Otlubel AU (SiO<sub>2</sub> 53–59 %, MgO 6.1–12.3 %, Al<sub>2</sub>O<sub>3</sub> 12.4–17.2 %, TiO<sub>2</sub> 0.2–0.4 %). The rare earth element (REE) and trace element patterns of the Holos AU are characterized by a strongly fractionated shape typical of ocean island basalts (OIB; Fig. 11c, d). On the multi-element variation plots normalized to primitive mantle, they do not show any negative Nb and Ta anomaly in line with their anorogenic nature.

In the Zr/Ti versus Nb/Y plot of Pearce (1996) the mafic rocks from the Holos AU lie in the alkali basalt, and those from the Otlubel AU in the basalt fields (Fig. 11b). However, the volcanic rocks from the Otlubel AU have high SiO<sub>2</sub> contents (SiO<sub>2</sub> 53–59%), which place them in the basaltic andesite and andesite fields in the total alkali – SiO<sub>2</sub> plot (not shown). They also have higher Mg numbers of 61–75 (molecular MgO\*100/(MgO + FeO<sub>total</sub>)) compared to the mafic rocks from the Holos AU (45–55), and lower concentrations of P<sub>2</sub>O<sub>5</sub> (0.01–0.003 wt %), Zr (7–15 ppm), Nb (1–2 ppm), Y (6–12 ppm), Th (0.3–0.6 ppm) and Hf (0.3–0.5 ppm) than the alkali basalts from the Holos AU (P<sub>2</sub>O<sub>5</sub> 0.22–1.04 wt %, Zr 98–429 ppm, Nb 16–85 ppm, Y 17–37 ppm, Th 2–35 ppm and Hf 3–11 ppm; Table 2). The magmatic rocks from the Otlubel AU show less enrichment in rare earths than average enriched and normal mid-ocean ridge basalt (E-MORB and N-MORB; Fig. 11c) and have a typical flattened concave-upward pattern (Fig. 11c), which is observed in boninites (e.g. Crawford & Cameron, 1985; Pearce *et al.* 1992). They also show minor depletion in Nb and Ta on multi-element variation plots normalized to primitive mantle, suggesting subduction influence. The mafic rocks from the Otlubel AU with their elevated SiO<sub>2</sub> (53–59%) and low TiO<sub>2</sub> (0.2–0.4%) contents, high Mg numbers (61–75) and REE pattern can be classified as boninites and plot in the boninite field of Pearce & Reagan (2019) (Fig. 11f).

In the Th/Yb versus Nb/Yb plot (Pearce, 2008), the Holos samples lie on the MORB–OIB array and close to the OIB field, whereas the Otlubel samples lie close to E-MORB but show a slight Th enrichment, which indicates a subduction influence (Fig. 11e). Only one basalt sample was analysed from the Kuyumcudağ AU, and it is geochemically similar to the alkali basalts from the Holos AU.

The plagiogranite sample is characterized by low K<sub>2</sub>O (0.41 wt %) and high Na<sub>2</sub>O contents (3.91 wt %; Table 2) and is chemically similar to oceanic plagiogranites (e.g. Coleman & Peterman, 1975). Its trace and rare earth element concentrations show a similar pattern to the mafic rocks of the Otlubel AU and are distinct from those of the Holos AU (Fig. 11c, d, e). This supports the view that the magmatic rocks of the Otlubel AU form a comagmatic sequence distinct from those of the Holos AU.

There are a large number of studies on the geochemistry of basaltic rocks from the ophiolitic mélanges in the Ankara region (e.g. Çapan & Floyd, 1989; Floyd, 1993; Tankut *et al.* 1998; Rojay *et al.* 2001, 2004; Gökten & Floyd, 2007; Göncüoğlu *et al.* 2010; Dangerfield *et al.* 2011; Sarıfakıoğlu *et al.* 2014, 2017; Bortolotti *et al.* 2018). These studies have shown that the dominant rock in the ophiolitic mélange is an ocean island type alkali basalt, similar to those from the Holos AU. This is also the case, for example, in the Japanese subduction-accretion complexes (e.g. Isozaki *et al.* 1990), and is explained by preferential accretion of topographic highs at the subduction zones. In the Ankara ophiolitic



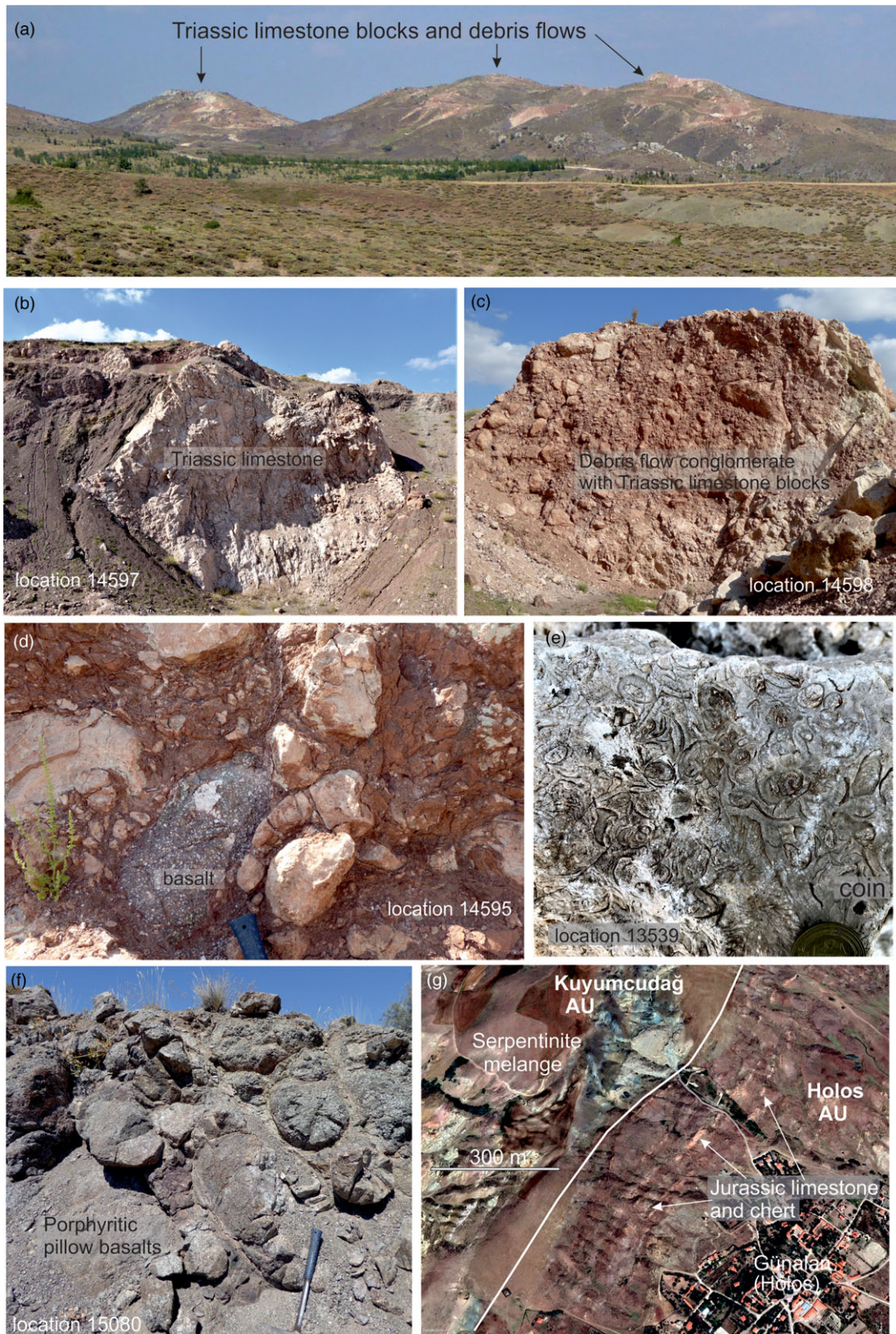


**Fig. 8.** (Colour online) Photographs of the shallow marine Upper Triassic limestone blocks in the Holos AU. (a) General view of the Triassic limestone blocks and debris flows. (b) A large block of Upper Triassic limestone encased in volcanoclastic matrix. (c) Debris flow conglomerate with Triassic limestone blocks. (d) Conglomerate with Upper Triassic limestone and basalt clasts. (e) Close-up view of the Upper Triassic limestone with corals and bivalves. (f) Pillow lavas of the Holos AU of porphyritic alkali basalt. (g) Detailed image showing the strong steep tectonic fabric in the Holos AU marked by the tectonic alignment of Jurassic pelagic limestone and chert. For the location of the image see Figure 4.



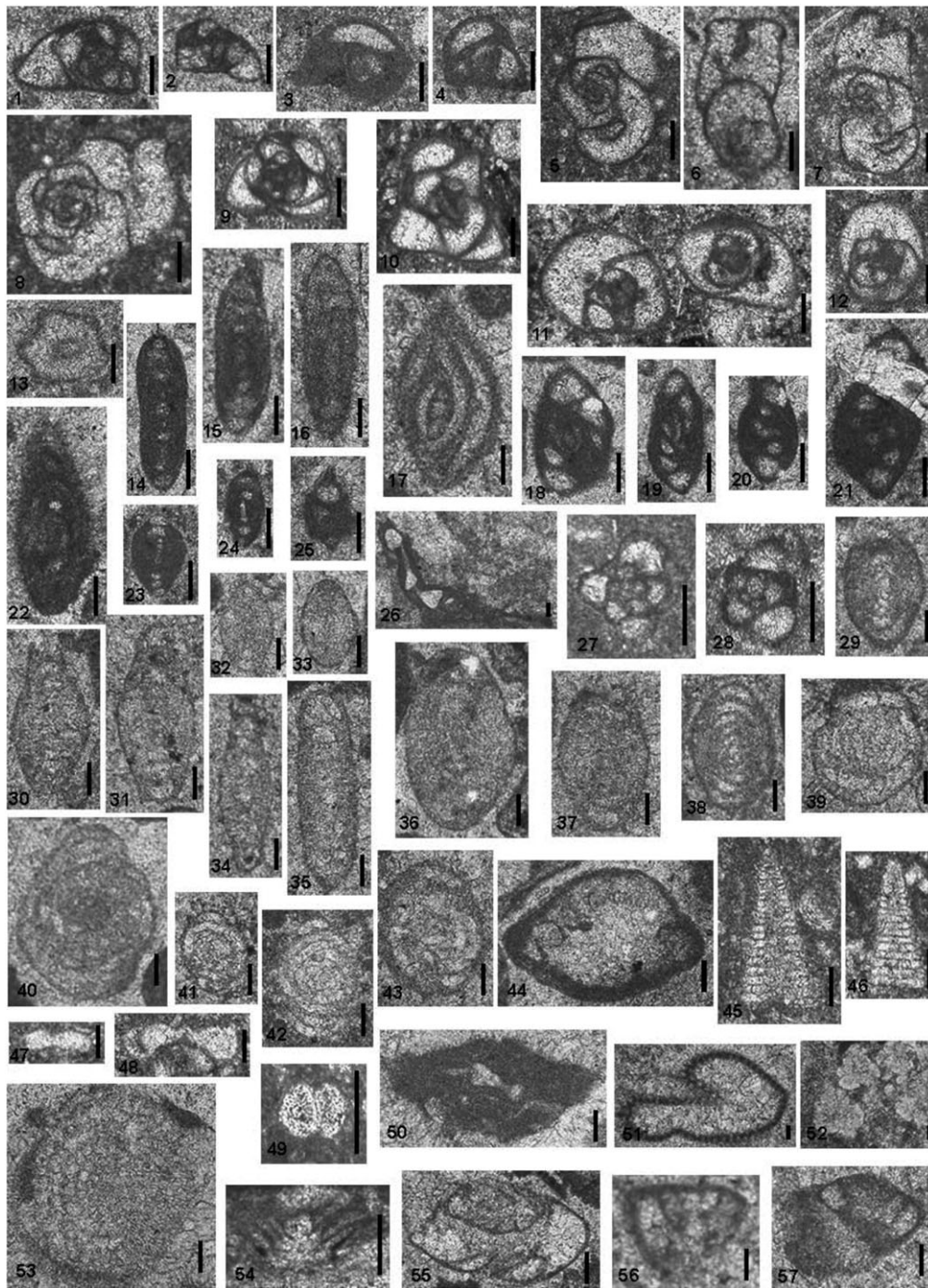


**Fig. 9.** Microphotographs of the foraminifera, algae and incertae sedis from the Upper Norian to Rhaetian blocks (Hörç Limestone) from the Beynam. **1–2.** *Galeanella? minuta* Zaninetti, Altiner, Dağ and Ducret. **3–4.** *Galeanella laticarinata* Al-Shaibani, Carter and Zaninetti. **5–8.** *Galeanella* sp. A. **9–12.** Galeanellid foraminifera. **13.** *Siculocosta floriformis* Zaninetti and Altiner? **14.** *Ophthalmidium leischneri* (Kristan-Tollmann). **15–16, 17?** *Ophthalmidium maximum* Zaninetti, Altiner, Dağ and Ducret. **18–21.** *Decapopolina schaeferae* (Zaninetti, Altiner, Dağ and Ducret). **22.** *Orthotrinaracia* sp. **23.** *Arenovidalina?* sp. **24.** *Ophthalmidium?* sp. **25.** *Miliolechina?* sp. **26.** *Nubecularia?* sp. **27–28.** *Miliolipora cuvillieri* Brönnimann and Zaninetti. **29, 36–38.** *Aulotortus* ex gr. *sinuosus* Weynschenk. **30–31.** *Aulotortus communis* (Kristan). **32–33.** *Triadodiscus eomesozoicus* (Oberhauser). **34.** *Aulotortus tumidus* (Kristan-Tollmann). **35.** *Aulotortus planidiscoides* (Oberhauser). **39.** *Parvalamella praegaschei* (Koehn-Zaninetti). **40–43.** *Parvalamella friedli* (Kristan-Tollmann). **44.** *Auloconus permodiscoides* (Oberhauser). **45–46.** *Trocholina ultraspirata* Blau. **47.** *Semiinvoluta* sp. **48.** *Kristantollmanna?* sp. **49.** *Globochaete* sp. **50.** *Tubiphytes obscurus* (Maslov). **51.** *Thaumtoporella parvovesiculifera* (Raineri). **52.** *Baccanella floriformis* Pant. **53.** *Triasina hantkeni* Majson. **54.** *Foliotortus spinosus* Piller and Senowbari-Daryan. **55.** *Diploremina?* sp. **56–57.** *Variostoma?* spp. 1–2, 5–8, 24, 45–46, 52, 54: sample 14639; 3–4, 25: sample 14595; 9–12, 23, 26, 47–48: sample 14596; 13: sample 15083; 14–17, 21–22, 37, 50, 53: sample 14591; 18–20, 32–33, 36, 40, 44: sample 14819; 27–28, 42: sample 14835; 29, 38, 57: sample 14820; 30–31, 34, 39, 41: sample 13537; 35, 43, 51, 56: sample 14817; 49: sample 14592; 55: sample 15537. Scale bar: 100  $\mu$ m.

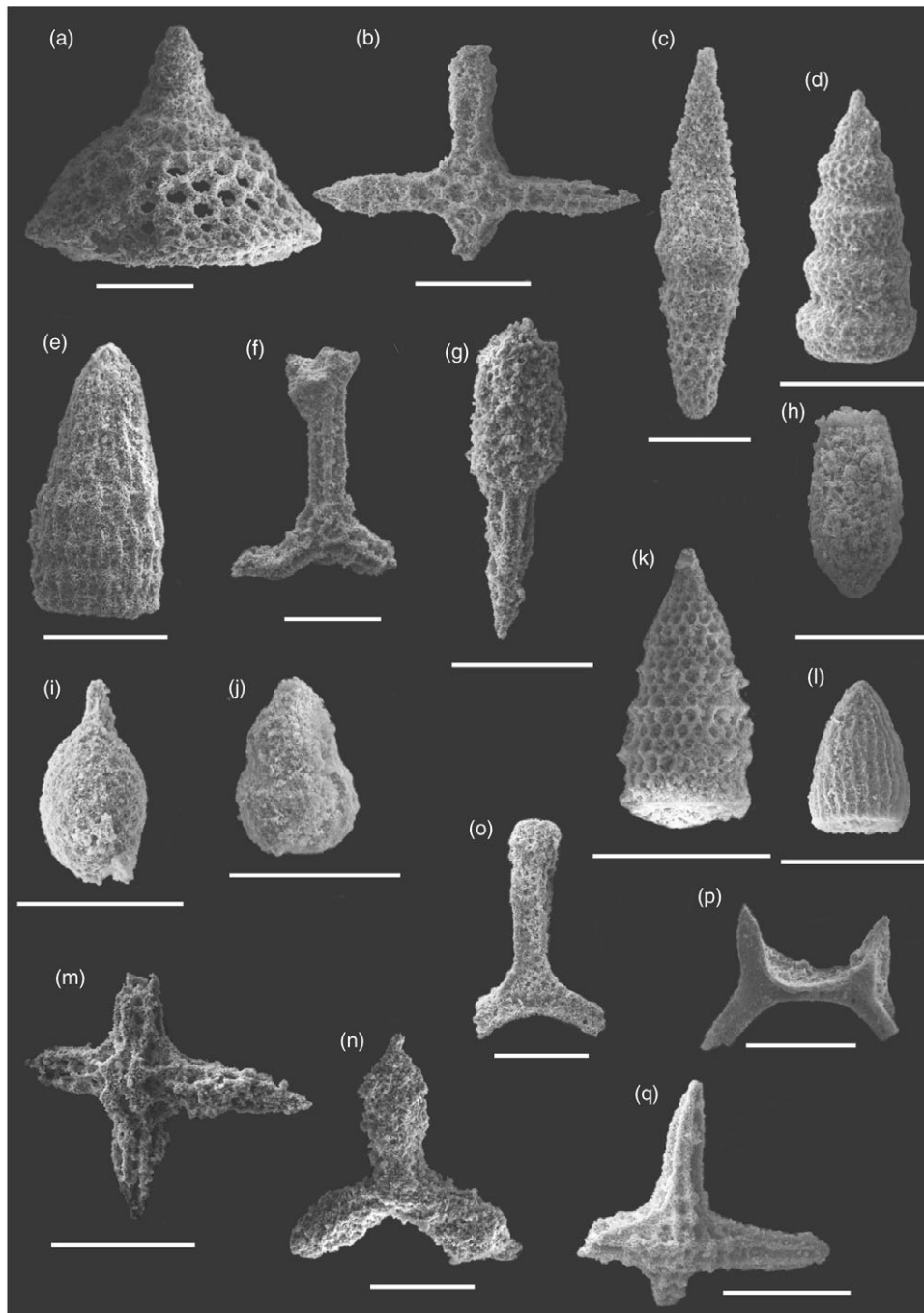


**Fig. 10.** Scanning electron microscope images of radiolaria from ribbon cherts from the Beynam area. (a) *Palinandromeda podbielensis* (Ozvoidova); (b) *Tetradytyma corralitosensis* (Pessagno) s.l.; (c) *Pseudoeucyrtis firma* Hull; (d) *Cinguloturris getsensis* O'Dogherty, Gorican and Dumitrica; (e) *Transhsuum maxwelli* (Pessagno) gr.; (f) *Tritrabs casmaliensis* (Pessagno); (g) *Archaeospongoprunum* sp. cf. *A. elegans* Wu; (h) *?Guexella nudata* (Kocher); (i) *Kilinora (?) oblongula* (Kocher); (j) *Theocapsommella* sp. cf. *T. medvednicensis* (Gorican); (k) *Triversus schardtii* O'Dogherty, Gorican and Dumitrica; (l) *Archaeodictyomitra patricki* Kocher; (m) *Archaeohagistrum munitum* Baumgartner; (n) *Paronaella mulleri* Pessagno; (o) *Angulobracchia digitata* Baumgartner; (p) *Hexasaturnalis nakasekoj* Dumitrica and Dumitrica-Jud; (q) *Emiluvia premyogii* Baumgartner. Sample 14585 (a–h), sample 14584 (i–l) and sample 15127 (m–q). Scale bar = 100  $\mu\text{m}$  for all specimens.

mélanges there are also smaller amounts of E-MORB and N-MORB type tholeiitic basalts locally with subduction influence (e.g. Rojay *et al.* 2004; Nairn *et al.* 2013; Bortolotti *et al.* 2018). In most cases there is no clear spatial or tectonic separation of different basalt types in the ophiolitic mélange. Dangerfield *et al.* (2011) notes the presence of three types of basalt in an area as small as 20 km<sup>2</sup>. However, in the Beynam case, different types of basalts

clearly belong to different subduction-accretion units. The Holos AU has alkali basalts, whereas Otlubel AU contains boninites, which appear to be rare in the Anatolian ophiolitic mélanges. Sarifakioğlu *et al.* (2017) describe boninites from the ophiolitic mélange in the Eldivan region, 110 km NE of Beynam (Fig. 2), and Robertson *et al.* (2013) from the southern margin of the easternmost Pontides.



**Table 2.** Geochemistry of mafic rocks and plagiogranite from the ophiolitic mélange, Beynam–Ankara region

Sample		13520	13521	13522	13524	14850	14855	13544	14716	14737	14833	14897	14899	14900	14845	
Rock type	Detect. limits	Gabbro	Diabase	Diabase	Diabase	Diabase	Plagiogranite	Porphyritic basalt	Analcime basalt	Diabase	Porphyritic basalt	Basalt	Porphyritic basalt	Basalt	Basalt	
AU		Otlu	Otlu	Otlu	Otlu	Otlu	Otlu	Holos	Holos	Holos	Holos	Holos	Holos	Holos	Holos	Kuy
Major oxides (wt %)																
SiO <sub>2</sub>	0.01	54.36	51.67	56.45	56.90	51.46	72.31	46.48	41.86	43.55	46.57	52.43	44.56	47.09	48.16	
TiO <sub>2</sub>	0.01	0.16	0.17	0.29	0.34	0.23	0.51	1.30	0.93	3.38	1.56	2.36	1.41	2.30	2.17	
Al <sub>2</sub> O <sub>3</sub>	0.01	16.84	13.31	11.85	12.60	13.44	12.85	19.69	12.52	15.28	18.15	15.62	17.62	15.25	15.76	
Fe <sub>2</sub> O <sub>3</sub>	0.01	7.52	7.86	6.81	8.64	13.91	2.85	5.08	11.71	10.96	8.90	8.41	5.26	11.20	10.59	
Cr <sub>2</sub> O <sub>3</sub>	0.002	0.027	0.119	0.143	0.096	0.068	0.019	0.014	<0,002	<0,002	0.015	0.003	0.009	0.009	0.014	
MnO	0.01	0.11	0.10	0.08	0.12	0.18	0.04	0.12	0.23	0.15	0.25	0.31	0.21	0.16	0.24	
MgO	0.01	5.97	11.55	10.25	8.50	11.44	1.16	2.71	6.88	4.26	5.39	3.42	3.06	4.72	3.51	
CaO	0.01	11.51	11.49	8.39	8.42	1.82	3.74	12.52	9.69	8.96	8.05	6.98	13.25	9.99	7.8	
Na <sub>2</sub> O	0.01	1.40	0.87	1.43	1.02	0.32	3.82	2.74	5.70	3.44	2.65	5.51	2.75	4.09	5.15	
K <sub>2</sub> O	0.01	0.12	0.03	0.09	0.05	<0,01	0.40	2.09	0.81	2.67	0.65	0.75	2.10	0.22	1.36	
P <sub>2</sub> O <sub>5</sub>	0.01	0.02	0.01	0.03	0.03	0.02	0.10	0.20	0.93	1.04	0.22	0.35	0.22	0.34	0.75	
LOI		1.80	2.70	4.00	3.20	6.70	2.10	6.90	8.30	5.90	7.40	3.60	9.40	4.40	4.20	
Sum		99.91	99.91	99.89	99.91	99.58	99.92	99.84	99.66	99.69	99.85	99.81	99.85	99.82	99.74	
Trace elements (ppm)																
Sc	1	51	49	37	40	49	18	22	23	17	27	33	23	31	16	
Ni	20	88.7	208.3	197.5	110.4	110	41.3	52.8	7.1	37.6	31.2	17.4	25.7	21.7	76.1	
Cu	0.1	3.1	4.6	4	2	2438	3.7	21	104	30.5	23.6	26.7	35.1	36.2	54.1	
Co	0.2	33.9	46	40.8	37	47.3	8.9	36.3	37.4	33.7	34.6	48.8	32.6	39.8	31.1	
Ga	0.5	15.4	9.5	9.5	10.5	11.7	11.1	17.2	10.5	19.5	20	16.8	17.4	18.4	21.8	
V	8	214	243	257	242	242	64	169	197	143	210	350	187	292	160	
Rb	0.1	1.4	0.2	1.2	0.5	<0,1	5.5	28.2	68	47.3	9.9	14.5	28.7	1	19	
Sr	0.5	96.1	81.4	151.3	70.9	45.5	134.1	399.7	1000	878.6	337.6	296.7	341.4	310.2	591	
Y	0.1	10.2	5.8	10	11.7	5.5	21.5	16.7	30	36.9	16.8	24.1	17.4	25.2	30.1	
Zn	1	3	5	11	8	150	6	44	79	120	58	108	50	75	102	
Zr	0.1	11.4	7.3	13.9	14.4	10.5	46	97.4	297.3	428.9	98.4	164.3	106.9	160.4	427.3	
Nb	0.1	1.2	1	1.5	1.4	1.2	3.8	17.7	16	85.3	17.7	27.9	17.9	26.6	54.2	
Cs	0.1	<0,1	<0,1	<0,1	<0,1	<0,1	0.3	0.4	5.9	<0,1	0.1	0.2	0.9	<0,1	<0,1	
Ba	1	31	32	36	16	5	15	295	1013	715	409	196	269	160	395	

(Continued)

**Table 2.** (Continued)

Sample		13520	13521	13522	13524	14850	14855	13544	14716	14737	14833	14897	14899	14900	14845
Rock type	Detect. limits	Gabbro	Diabase	Diabase	Diabase	Diabase	Plagiogranite	Porphyritic basalt	Analcime basalt	Diabase	Porphyritic basalt	Basalt	Porphyritic basalt	Basalt	Basalt
AU		Otlu	Otlu	Otlu	Otlu	Otlu	Otlu	Holos	Holos	Holos	Holos	Holos	Holos	Holos	Kuy
Hf	0.1	0.4	0.3	0.5	0.5	0.3	1.3	2.5	7.9	10.9	2.5	3.9	2.5	4.1	9
Ta	0.1	<0,1	<0,1	<0,1	0.1	<0,1	0.3	1	0.8	5.6	1	1.7	1.1	1.7	3.2
Pb	0.1	0.1	<0,1	0.2	<0,1	0.6	0.2	0.6	41.1	2.9	0.6	1	0.8	1.7	6.6
Th	0.2	0.4	0.3	0.6	0.4	0.3	1.3	2.1	34.9	8.2	2.1	3.4	2.1	3.1	9.5
U	0.1	<0,1	<0,1	0.1	0.2	0.1	0.5	0.7	8.4	1.2	0.4	0.9	0.5	0.7	2.9
Rare earth elements (ppm)															
La	0.1	1.7	1.3	2.3	1.8	1.4	3.8	16.3	108.2	78.4	16	23.6	15.9	24.4	63.6
Ce	0.1	2.8	1.9	3.2	2.8	1.1	7.2	31.6	223.2	160.4	30.9	49.6	31.7	47.9	119.3
Pr	0.02	0.35	0.19	0.33	0.31	0.13	0.86	3.88	27.24	19.91	3.84	6.05	3.92	5.92	13.48
Nd	0.3	1.3	0.8	1.3	1.4	0.5	4.4	15.6	106.2	80.8	15.3	24.2	16	24	50.3
Sm	0.05	0.44	0.25	0.44	0.54	0.25	1.37	3.27	20.09	15.23	3.47	5.13	3.36	5.3	9.12
Eu	0.02	0.16	0.11	0.22	0.22	0.09	0.47	1.23	4.76	4.57	1.27	1.77	1.25	1.79	2.51
Gd	0.05	0.9	0.52	0.86	1.04	0.53	2.46	3.57	15.28	12.89	3.62	5.53	3.7	5.66	8.19
Tb	0.01	0.21	0.11	0.2	0.22	0.12	0.46	0.55	1.76	1.73	0.57	0.86	0.59	0.85	1.15
Dy	0.05	1.47	0.93	1.55	1.82	0.81	3.26	3.03	7.31	8.63	3.15	4.9	3.33	4.91	6.22
Ho	0.02	0.4	0.22	0.39	0.46	0.23	0.81	0.65	1.06	1.43	0.64	0.96	0.67	0.96	1.17
Er	0.03	1.26	0.78	1.3	1.48	0.73	2.55	1.72	2.56	3.44	1.77	2.63	1.94	2.68	3.09
Tm	0.01	0.21	0.12	0.21	0.22	0.11	0.4	0.24	0.32	0.43	0.26	0.38	0.26	0.36	0.4
Yb	0.05	1.38	0.86	1.42	1.58	0.78	2.59	1.55	1.98	2.52	1.49	2.22	1.66	2.31	2.52
Lu	0.01	0.25	0.14	0.22	0.26	0.15	0.44	0.23	0.28	0.33	0.23	0.33	0.25	0.34	0.37



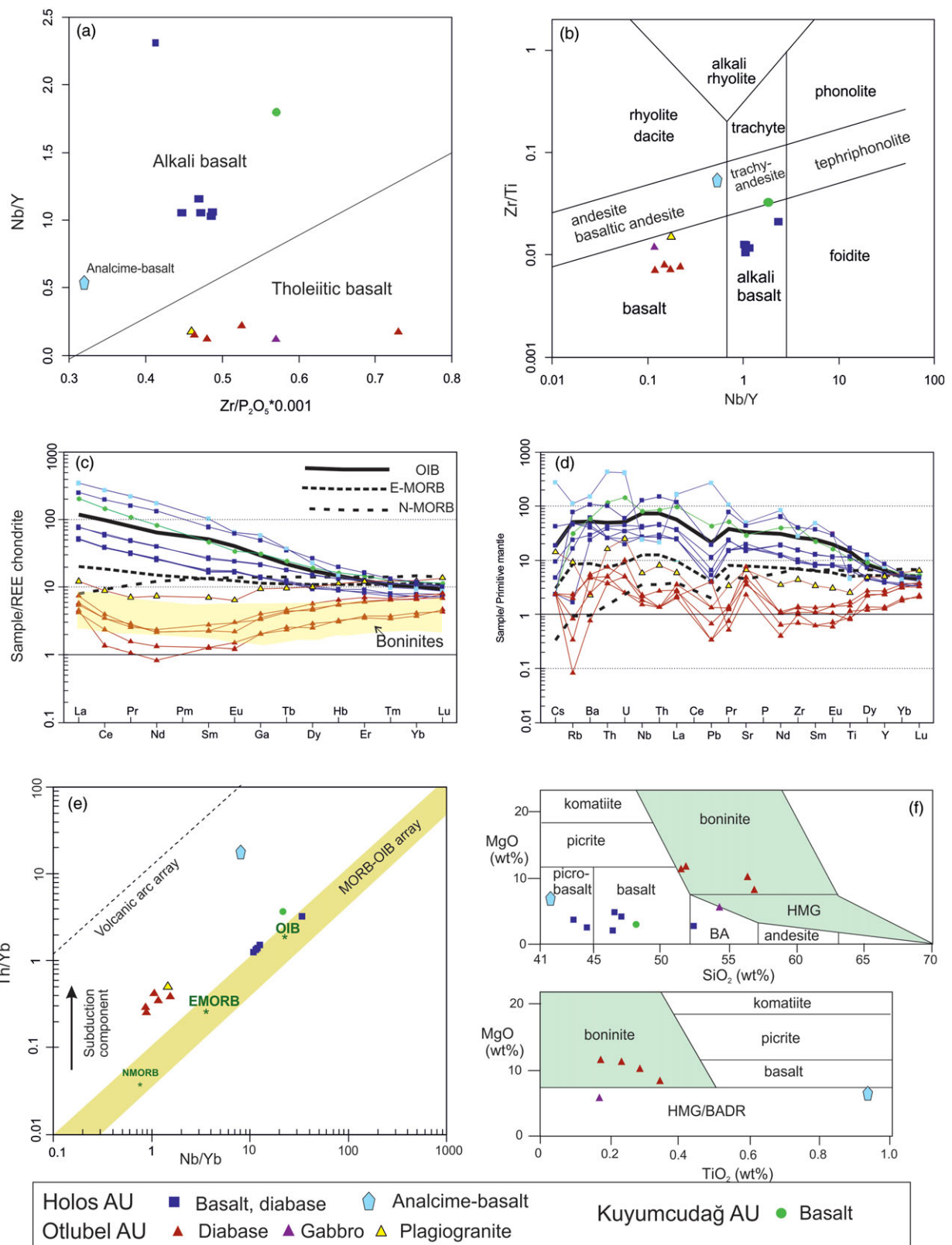


**Fig. 11.** (Colour online) Geochemical plots for the basaltic rocks and plagiogranite from the Beynam area. (a) Nb/Y versus  $Zr/P_2O_5 \cdot 0.001$  plot of Winchester & Floyd (1977). (b) Zr/Ti versus Nb/Y plot of Pearce (1996). (c) Chondrite-normalized REE patterns. Normalizing values from Boynton (1984). The light yellow strip shows REE values from boninites with data from Crawford & Cameron (1985) and Pearce et al. (1992). (d) Primitive-mantle-normalized trace element patterns. Normalizing values from McDonough & Sun (1995). (e) Th/Yb versus Nb/Yb plot after Pearce (2008). (f) Boninite classification plots after Pearce & Reagan (2019). The average OIB, E-MORB and N-MORB values shown in (b) and (c) are from Sun & McDonough (1989). HMA, high-Mg andesite; BADR, basalt-andesite-dacite-rhyolite series.

## 7. Upper Cretaceous fore-arc sequence: the Haymana Formation

The Holos AU is stratigraphically overlain by a thick sequence of Upper Cretaceous turbidites of the Haymana Formation. Upper Cretaceous turbidites have a wide distribution in central Anatolia and have been interpreted as a fore-arc sequence (Fig. 2; Görür et al. 1984; Koçyiğit, 1991; Nairn et al. 2013; Gülyüz et al. 2019). The Haymana Formation lies mostly on continental crustal sequences of the Sakarya Zone, including over the Upper Cretaceous limestones and olistostromes (Fig. 3; Ünalán et al. 1976; Okay & Altuner, 2016; Okay et al. 2019). Although some authors indicate a stratigraphic contact between the ophiolitic mélangé and the Upper Cretaceous turbidites (e.g. Norman, 1972; Ünalán, 1981; Akyürek et al. 1997; Nairn et al. 2013), there is no detailed description of such a contact. The Beynam region is one of the few places in the Ankara region where the stratigraphic contact between the ophiolitic mélangé and the fore-arc sequence is well exposed. Two detailed sections were measured across this contact (Fig. 12).

At the base of section-1, there are sheared basalt, radiolarian chert and pelagic shale. This is overlain by a coherent stratigraphic sequence of red radiolarian cherts intercalated with shale and basalt and rare pelagic limestone, 100 m in thickness (Fig. 12). Two samples of radiolarian cherts contain Middle to Late Jurassic (Bathonian–Oxfordian) radiolaria including *Kilinora* (?) *oblongula*, *Palinandromeda podbielensis* and ? *Guexella nudata* (Fig. 10). The Haymana Formation starts above this Jurassic oceanic crustal slice with a 12 m thick, massive conglomerate (Figs 11 and 12a, b). The conglomerate contains rounded, 1–5 cm large clasts of black marble, basalt, neritic limestone, serpentinite and diabase in a sandy matrix. A sample from a limestone clast contains Jurassic incertae sedis *Crescentiella morronensis*. The conglomerate is overlain by violet, red and green silty clayey marls (Figs 12 and 13c), which contain early to middle Campanian (~83–79 Ma) planktonic foraminifera *Globotruncanita elevata*, *Globotruncana linneiana*, *G. bulloides*, *G. arca*, *Planoheterohelix globulosa* and *Muricohedbergella* spp. (Fig. 7, photos 54–67). The marls are overlain by the typical thickly bedded, brown volcanogenic sandstones and shales of the Haymana Formation (Figs 12 and 14d).

At the base of section-2 there are also sheared, red radiolarian chert, red shale, basalt, red pelagic shale and rare serpentinite. Here, the Haymana Formation starts with medium, thickly bedded to massive, locally laminated volcanogenic sandstones, c. 20 m thick (Figs 12 and 13d), which lie unconformably over the ophiolitic mélangé. The sandstones are overlain by violet, red mudstone and red radiolarian cherts, which are followed by a second horizon of 45 m thick volcanogenic sandstone with mudstone and siltstone layers. Samples from the mudstones contain *Muricohedbergella planispira*, *Macroglobigerinolloides* sp. and radiolaria, which indicate a post-Aptian age. The poorly sorted sandstones are rich in large feldspar and quartz grains and lithic volcanic clasts (see Supplementary Material available online at <https://doi.org/10.1017/S0016756822000504>). A sandstone sample (11169) was analysed for detrital zircons. The zircon U–Pb age spectrum is shown in Figure 14b, and the isotopic data and the CL images of the zircons are given in Table S1 and Figure S1, respectively (see Supplementary Material). The Upper Cretaceous detrital zircons are predominantly euhedral and show igneous zoning (Fig. S1), and their Th/U ratios are above 0.2 (Table S1), which indicate an igneous origin (see Supplementary Material). Out of 118 zircons analysed, 47 were concordant at 90–100 %, and 30 of those are Santonian to early Campanian (81–87 Ma). The oldest ages (87 ± 3 Ma and 86 ± 3

Ma) are represented by single zircons each, whereas there are five zircons with 85 ± 3 Ma ages. The youngest detrital zircons are 81 ± 3 Ma (three zircons) and provide an early Campanian lower age limit for the Haymana Formation.

The Campanian volcanogenic sandstones are stratigraphically overlain by two conglomerate beds, 5 to 15 m in thickness, separated by volcanogenic sandstones (Fig. 12). The conglomerates consist of rounded, 1–5 cm large clasts of black marble, basalt, limestone, serpentinite and diabase in a sandy matrix. Limestone clasts from the conglomerate contain benthic foraminifera *Crescentiella morronensis*, *Mohlerina basiliensis* and *Charentia* sp. (Fig. 7, photos 69–71) characteristic of the Upper Jurassic – Lower Cretaceous. In terms of facies, lithology and fauna, the limestone clasts in the conglomerate are similar to those of the Bilecik Group of the Sakarya Zone (Fig. 3; Altuner et al. 1991). The conglomerates are in turn overlain by purple, green silty marls with a middle Campanian to middle Maastrichtian foraminiferal fauna including *Globotruncana linneiana*, *Gl. ventricosa* and *G. bulloides*, which pass up into volcanogenic sandstone and shale, which constitute the typical lithology of the Haymana Formation (Ünalán et al. 1976; Okay & Altuner, 2016). Sandstones from the Haymana Formation are generally poorly sorted greywackes rich in volcanic and plutonic clasts and their petrography indicates a magmatic arc provenance (Çetin et al. 1986).

In the Beynam region the Haymana Formation has a stratigraphic thickness in excess of 1 km. The predominant facies is an intercalation of volcanogenic sandstone and shale (Fig. 14d). The sandstones show typical turbidite features including graded bedding, parallel and convolute lamination and slumps. There is also a 40 m thick channelized debris flow horizon NE of the village of Günalan with poorly sorted clasts of basalt (Fig. 4). Within the sandstone–shale sequence, there are rare (<3 %) marl and calc-arenite beds; several samples from such beds contain planktonic foraminifera of middle Campanian to middle Maastrichtian age range including *Globotruncana linneiana*, *G. lapparenti*, *G. bulloides*, *G. arca*, *Muricohedbergella monmouthensis* and *Heterohelix globulosa* (Fig. 7, photos 58, 67) and also transported benthic foraminifera *Orbitoides* sp. and *Lepidorbitoides* sp.

Palaontological and isotopic data show that: (a) the base of the fore-arc sequence (the Haymana Formation) is early to middle Campanian in age (c. 81 Ma), which provides an upper age limit for the tectonic assembly of the AUs in the Beynam area, and (b) the fore-arc basin was sourced from Santonian to early Campanian (87–81 Ma) magmatic arc and from the ophiolitic mélangé. However, there is no indication that the ophiolitic mélangé was subaerially exposed prior to the deposition of the Haymana Formation. The prominent conglomerate levels in the base of the Haymana Formation represent debris flows, and the absence of volcanogenic sandstones in section-1 is most probably due to scouring by the massive debris flow.

## 8. Eocene sequence

The Haymana Formation is overlain with an angular unconformity by an Eocene shallow marine to continental sequence of sandstone, limestone and gypsum (Fig. 4). The Eocene sequence starts with sandy, pebbly limestones very rich in large benthic foraminifera. Individual foraminifera and rock samples, collected from the base of the Eocene section, yielded a shallow marine benthic foraminifera fauna including *Nummulites* ex. gr. *perforatus*, *Nummulites* spp., *Asterocyclina alticostata*, *Asterocyclina* sp., *Discocyclina* sp., *Orbitoclypeus* sp., *Asterigerina* sp. and *Victoriella* sp. (Fig. S2 in the Supplementary Material available



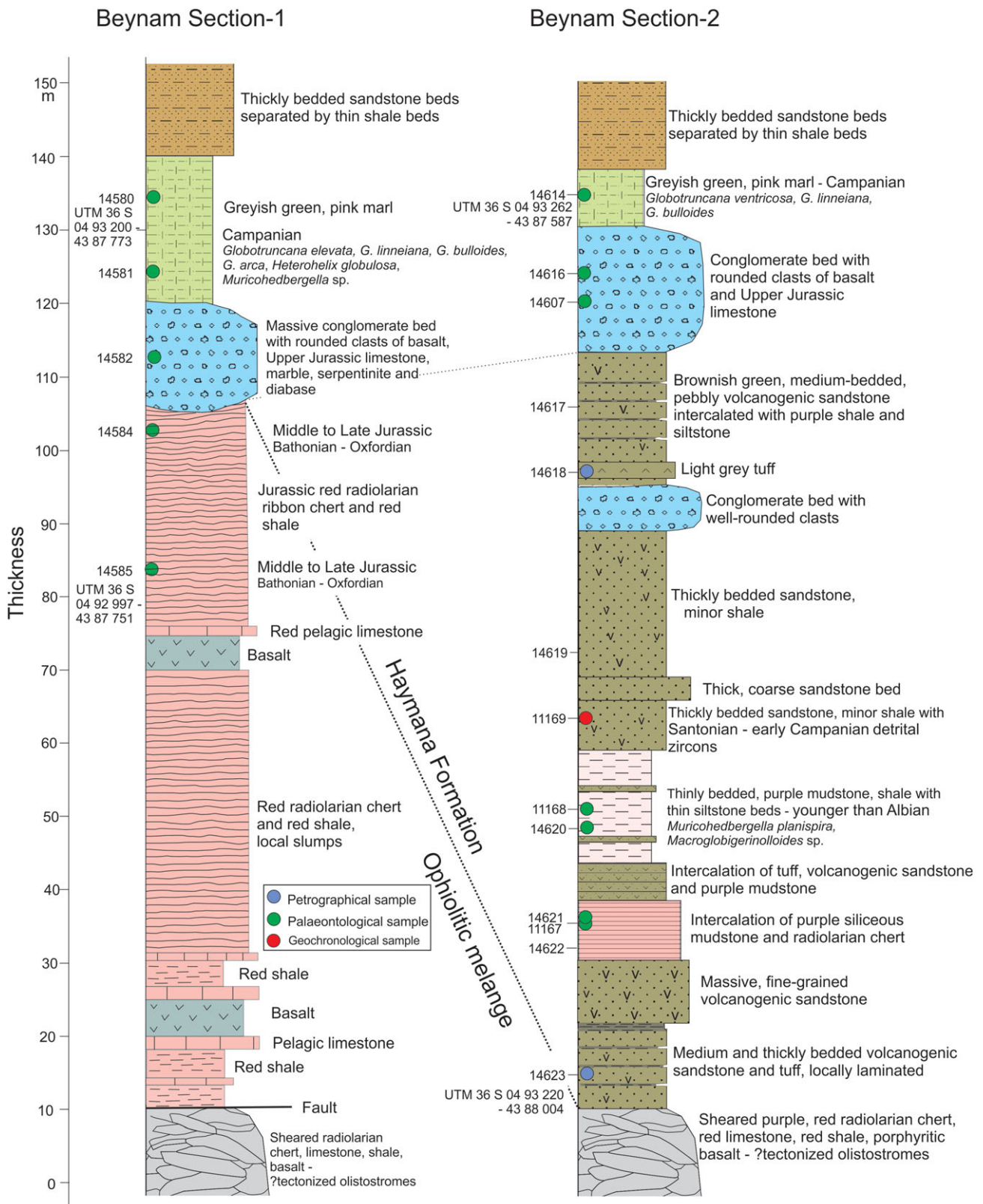


**Fig. 12.** (Colour online) Measured stratigraphic sections between the ophiolitic mélange (Holos AU) and the overlying fore-arc sequence of the Haymana Formation. The base of section-1 consists of a sheared mélange, which is tectonically overlain by a coherent Jurassic oceanic crustal sequence 95 m thick, which is in turn stratigraphically overlain by the fore-arc sediments of the Haymana Formation. In section-2 the fore-arc sequence (Haymana Formation) lies stratigraphically over the sheared ophiolitic mélange. For locations of the sections see Figure 4.



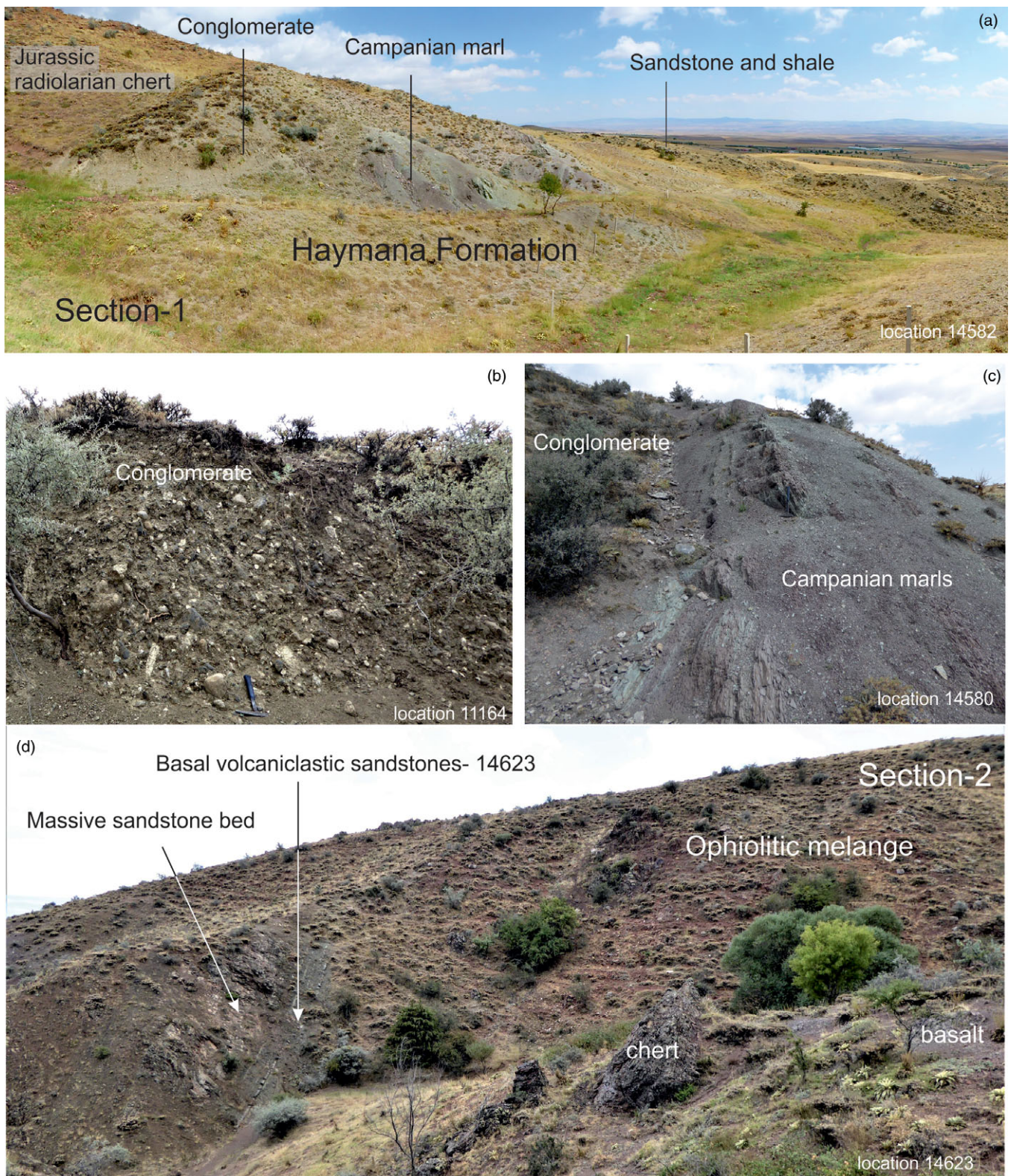


**Fig. 13.** (Colour online) Photographs from the Upper Cretaceous Haymana Formation and the stratigraphically underlying ophiolitic mélangé. (a) Jurassic radiolarian chert overlain stratigraphically by the Haymana Formation consisting of conglomerate, Campanian marl and sandstone–shale in section-1. (b) Campanian conglomerate with rounded clasts of basalt, diabase and limestone. (c) Campanian marls overlying the conglomerate. (d) Volcanoclastic sandstones of the Haymana Formation lying stratigraphically over the ophiolitic mélangé in section-2.



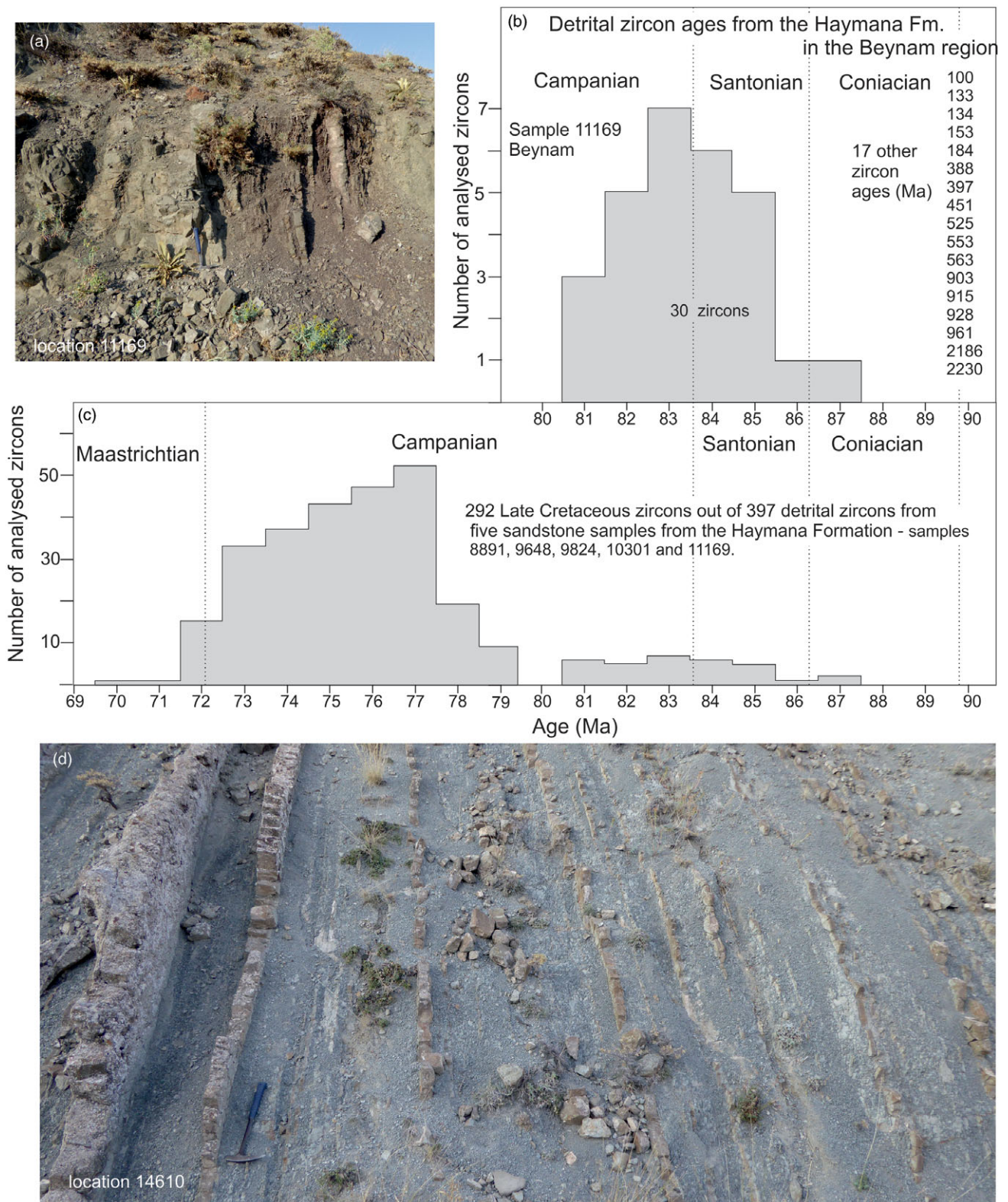


**Fig. 14.** (Colour online) (a–b) Detrital zircon U–Pb ages from a sandstone sample from the base of the Upper Cretaceous Haymana Formation, the fore-arc sequence; (a) shows the sample location. (c) Late Cretaceous detrital zircon ages from five sandstone samples from the Haymana Formation. For locations of the samples see Figure 2 and Okay *et al.* (2020a). (d) Turbiditic sandstones and shales of the Haymana Formation.

online at <https://doi.org/10.1017/S0016756822000504>). The fauna indicates a Middle Eocene age (middle–late Lutetian to early Bartonian). Considering that there are no marine Bartonian deposits in central and northern Anatolia (Okay *et al.* 2020b), the basal Eocene transgression can be dated to middle–late Lutetian (*c.* 45 Ma). Middle Eocene sandstones lie unconformably over the older units both in the Sakarya Zone and in the Kırşehir Massif (e.g. Gülyüz *et al.* 2013; Nairn *et al.* 2013; Okay *et al.* 2020b) and represent the oldest post-collisional cover.

## 9. Discussion

### 9.1 Accretionary units and boninites in the ophiolitic mélange

Geological mapping has shown that the ophiolitic mélange in the Beynam region consists of three AUs, distinguished by lithology, structure, age and geochemistry. The Kuyumcudag AU is the only one which can be defined strictly as a tectonic mélange (e.g. Raymond, 1984; Festa *et al.* 2020), in that it has a well-defined matrix of sheared serpentinite with blocks of basalt, Jurassic chert and limestone. The Otlubel AU is a semi-intact piece of Late Jurassic oceanic crust with boninite chemistry. The Holos AU is an imbricate tectonic stack of alkali basalt, chert and limestone. Accretionary units with similarly distinct lithological, geochemical, structural and temporal features are also described from the Franciscan Complex (e.g. Wakabayashi, 2015; Raymond *et al.* 2020) and from Japan (e.g. Isozaki *et al.* 1990; Isozaki, 1997).

While it is easy to explain the presence of alkali basalts in the Holos AU, as having formed on an oceanic seamount, the presence of boninites in the Otlubel AU poses a problem. Boninites are typically found in supra-subduction ophiolites, are commonly associated with subduction initiation and are located in the upper plate in a subduction system (e.g. Crawford *et al.* 1989; Pearce & Reagan, 2019). The Late Jurassic Otlubel AU is located in a subduction-accretion complex sandwiched between two other AUs, and thus was clearly part of the lower plate. However, it could have formed above a mid-oceanic subduction zone, and later been incorporated in the subduction-accretion complex (Fig. 15), as discussed in Section 9.5 further below.

### 9.2. Origin of the Triassic limestone blocks and debris flows

A number of observations indicate that the Triassic limestones in the Holos AU were deposited on an oceanic seamount, as also suggested by Sarifakioğlu *et al.* (2017). These observations include: (a) Lack of continent-derived siliciclastic detritus in the Holos AU, showing that the Triassic limestone blocks could not have been derived from a continent. (b) In the debris flows Triassic limestone and basalt blocks are closely intermixed (Fig. 8d), suggesting that the Hörç limestone was deposited on oceanic basalt. (c) The geochemistry of the basalts in the Holos AU suggests an oceanic island setting. (d) The Hörç limestone is predominantly shallow marine. (e) The lithology and fauna of the Triassic limestones in the Holos AU are unique and cannot be correlated with any of the Triassic limestone sequences in the Pontides.

Seamounts and islands consisting of shallow marine limestone on a basaltic substratum are common in the present Pacific Ocean (Nunn *et al.* 2016). Accreted seamounts are common in the western Pacific convergent margins (e.g. Dilek & Ogawa, 2021), and shallow-marine limestone blocks including Late Triassic ones are described from subduction-accretion complexes in Japan (e.g. Isozaki *et al.* 1990; Chablais *et al.* 2010). The collapse of the limestone carapace occurs during the attempted subduction of the

seamount (e.g. Sano & Kanmera, 1991). The Hörç Limestone must also have been deposited on a Triassic oceanic seamount in the Tethyan ocean, and then been incorporated into an accretion complex during the subduction (Fig. 15a, b).

### 9.3. The age of the subducting Tethyan oceanic lithosphere: Triassic to Early Cretaceous

Continent-derived sediments are absent in the ophiolitic mélange in the Beynam region, therefore all rocks in the ophiolitic mélange must have been formed or deposited on oceanic crust. Palaeontological and isotopic data from the ophiolitic mélange in the Beynam region indicate the presence of Triassic and Late Jurassic oceanic crust. The oceanic seamount recorded in the Holos AU must have been constructed on a pre-Late Triassic oceanic crust. Further support for the presence of a Triassic oceanic crust in the İzmir–Ankara ocean is found in the ophiolitic mélanges further west, in the Mihaliçcik region, which include Upper Triassic radiolarian cherts (Tekin *et al.* 2002), and further east in the Late Triassic plagiogranites (*c.* 225 Ma; Çelik *et al.* 2018). The age of the plagiogranite and the ages of sedimentary rocks in the Beynam region, including radiolarian cherts, provide solid data for the Jurassic oceanic crust. Similar Jurassic ages are reported from other parts of the ophiolitic mélange in the Ankara region (Dilek & Thy, 2006; Çelik *et al.* 2011; Sarifakioğlu *et al.* 2017; Bortolotti *et al.* 2018) and further east in the Eastern Pontides (Topuz *et al.* 2013; Robertson *et al.* 2013) and Lesser Caucasus (Danelian *et al.* 2010, 2016; Rolland *et al.* 2010). The youngest rocks in the Beynam area are Lower Cretaceous pelagic limestones.

Published ages of radiolaria and foraminifera from the oceanic sedimentary rocks in the ophiolitic mélanges in central Anatolia range from Late Triassic (late Norian) to early Late Cretaceous (Cenomanian, *c.* 100 Ma; Fig. 3). There are no confirmed post-early Late Cretaceous palaeontological ages from the ophiolitic mélange, which suggests that the subducting oceanic lithosphere was Triassic to early Late Cretaceous in age. The radiolarian chert sequences described from the ophiolitic mélanges also have short age ranges (Fig. 3), which implies a short period between the generation of oceanic lithosphere and its subduction.

### 9.4. Separating subduction-related and collision-related deformations

The Late Cretaceous subduction of the İzmir–Ankara ocean was followed by the Palaeocene hard collision between the Sakarya Zone and the Kırşehir Massif (e.g. Kaymakçı *et al.* 2009; Meijers *et al.* 2010; Lefebvre *et al.* 2013). The architecture of the ophiolitic mélange in the Ankara region is therefore the combined result of subduction and collision. The preservation of the Upper Cretaceous fore-arc turbidites, the Haymana Formation, in the Beynam region allows a separation between these two types of structures. The Haymana Formation is characterized by sub-vertical dips but does not show any small-scale folding or disruption of bedding in the Beynam area, where it is overlain unconformably by Middle Eocene sedimentary rocks. This shows that the steep tectonic fabric in the ophiolitic mélange and in the Haymana Formation is a result of continental collision. The Palaeocene collision in central Anatolia was not intense since the ongoing convergence between Eurasia and the Arabian Platform was partly taken up by subduction along the Eastern Mediterranean and the Bitlis–Zagros ocean (Fig. 1b). In the Haymana region, which was located further away from the trench than the Beynam area (Fig. 2), the marine sedimentation continues without a break from



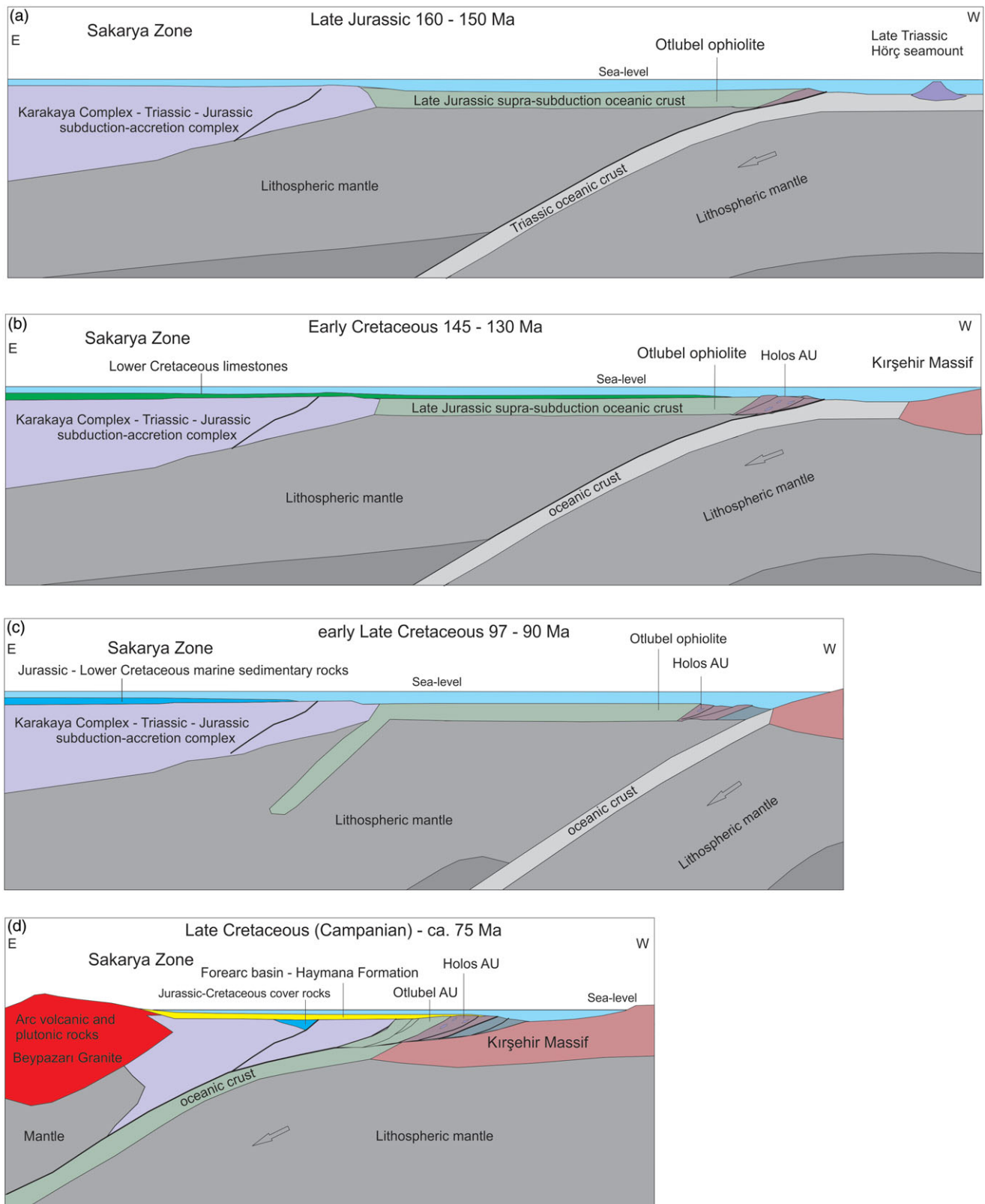


**Fig. 15.** (Colour online) Schematic diagrams illustrating Jurassic–Cretaceous evolution of the Ankara region. (a) During the Late Jurassic, the Otlubel ophiolite forms in an intra-oceanic supra-subduction setting. (b) The accretion of Triassic and Jurassic oceanic crust, including Late Triassic seamounts and Middle Jurassic cherts, continues during the Early Cretaceous during which limestone deposition extends from the continent to the ocean. (c) During the early Late Cretaceous the subduction zone jumps inboard, possibly triggered by the soft collision with the Kırşehir Massif. (d) In the Late Cretaceous, Andean-type subduction results in the formation of a magmatic arc and leads to the development of a fore-arc basin, which covers the earlier-formed AUs. The Otlubel AU is accreted during this period.

the Late Cretaceous into the Middle Eocene (e.g. Ünalın *et al.* 1976; Kaymakçı *et al.* 2009; Nairn *et al.* 2013).

Restoration of the bedding in the Haymana Formation to the horizontal results in a sub-horizontal fabric in the ophiolitic mélangé similar to that observed in frontally accreted subduction-accretion complexes. Frontal accretion is also compatible with the lack of high-pressure metamorphism in the ophiolitic mélangé in the Ankara region. The ophiolitic mélangés in the Tavşanlı Zone further west show an incipient HP metamorphism with the development of lawsonite, aragonite, sodic amphibole and sodic pyroxene (Topuz *et al.* 2006; Plunder *et al.* 2013), which are not found in central Anatolia.

### 9.5. Mesozoic evolution

Pontides have been an active margin at least since the Triassic. However, subduction accretion and arc magmatism have been episodic, with major phases during the Late Triassic, Middle Jurassic (175–155 Ma) and Late Cretaceous (e.g. Fig. 3; Okay & Nikishin, 2015; Akdoğan *et al.* 2018, 2019; Okay *et al.* 2019). The Late Jurassic – Early Cretaceous (157–135 Ma), on the other hand, was a period of carbonate deposition in the Pontides, with little evidence for arc magmatism or subduction accretion. However, data from the Beynam region suggest that subduction was initiated during the Late Jurassic (*c.* 161 Ma), leading to the formation of a supra-subduction oceanic lithosphere, as represented by the boninitic Otlubel AU (Fig. 15a). The surface of the newly created oceanic crust must have been above the carbonate-compensation depth as shown by the deposition of the pelagic carbonates, which also characterize the Upper Jurassic – Lower Cretaceous stratigraphy of the Sakarya Zone (Fig. 3; Altner, 1991). This suggests that pelagic carbonate deposition extended from the continental margin to the supra-subduction oceanic crust (Fig. 15a). Robertson *et al.* (2021) describe a similar situation from the ophiolitic mélangé in the Aladag region in the Taurides. The interaction between the pelagic carbonates and Late Jurassic volcanism may have formed the debris-flow conglomerates observed in the Otlubel AU. The accretion of the Holos AU most probably occurred during the Late Jurassic – Early Cretaceous in this intra-oceanic subduction zone, which involved collision and partial accretion of the Hörç seamount (Fig. 15a).

The incorporation of the Late Jurassic supra-subduction oceanic crust in the subduction-accretion complex requires that in the early Late Cretaceous the subduction zone jumped inboard to the ocean–continent boundary, resulting in an Andean-type subduction zone (Fig. 15b; Dangerfield *et al.* 2011). This might have been initiated through soft collision with the Kırşehir Massif (Fig. 15c). This also led to the development of a continental magmatic arc and of a fore-arc basin (Fig. 15c). This Palaeogalatian arc, first suggested by Koçyiğit (1991), is mainly represented by the Late Cretaceous (80–73 Ma) I-type Beypazarı Granite with a geochemistry compatible with a magmatic arc setting (Öztürk *et al.* 2012) and a few outcrops of Upper Cretaceous volcanic rocks (Fig. 2; Koçyiğit *et al.* 2003; Okay *et al.* 2019); most of it is concealed under the Neogene sedimentary cover (Fig. 2).

The time of initiation of the Andean-type subduction zone can be estimated from the timing of continental arc magmatism, the best record of which is found in the fore-arc basin sediments (e.g. Paterson & Ducea, 2015; Sharman *et al.* 2015), represented in this case by the Haymana Formation. In the Beynam region, detrital zircons from the basal sandstone beds of the Haymana Formation are predominantly Santonian to Campanian (87–81 Ma; Fig. 14b),

suggesting *c.* 87 Ma for the start of arc magmatism. Further east, in the Haymana and Alcı areas, the detrital zircons from the Haymana Formation are younger mostly Campanian to early Maastrichtian (80–71 Ma; Fig. 14c; Okay *et al.* 2019). This indicates that Late Cretaceous arc magmatism ranged between 87 Ma and 71 Ma (Santonian – early Maastrichtian). The time between the initiation of subduction and inception of arc magmatism depends on the slab dip angle and convergence rate, and ranges from a few million to 10 million years (e.g. Stern, 2002). The well-dated Coniacian (89–87 Ma) olistostromes in the Sakarya Zone (Fig. 2) contain clasts of ophiolitic mélangé, which must have been derived from an accretionary complex (Okay *et al.* 2019). These constrain the inception of Andean-type subduction to Cenomanian–Turonian (*c.* 97–90 Ma; Fig. 15c). Hence, the incorporation of the Otlubel AU in the ophiolitic mélangé must have occurred during the Late Cretaceous. The Late Cretaceous subduction zone in the Ankara region had a NNE trend, which was also suggested for the western boundary of the Kırşehir Massif (Lefebvre *et al.* 2013; van Hinsbergen *et al.* 2016; Maffione *et al.* 2017).

### 9.6. Lack of land-derived sandstones in the subduction-accretion units

All large subduction-accretion complexes, such as the Franciscan Complex in California or the Makran Complex in Iran, are dominated by greywacke-type sandstones derived from the magmatic arc and deposited in the trench and fore-arc. In contrast, no sandstones are recognized in the ophiolitic mélangé in the Beynam region; in other parts of Anatolia, sandstones generally make up a few per cent of the ophiolitic mélangé (e.g. Plunder *et al.* 2013; Okay *et al.* 2020a). Detrital zircons from the rare sandstone bodies in the ophiolitic mélangé west of Ankara do not contain any Jurassic or Cretaceous zircons (Okay *et al.* 2020a). The absence of sandstones in the Anatolian ophiolitic mélangés can be ascribed to three factors: (a) The main phase of accretion took place during the Late Jurassic – Early Cretaceous in an intra-oceanic subduction zone away from continental influence. (b) The Late Jurassic – Early Cretaceous was a period of marine limestone deposition on the continent, on the Sakarya Zone (Figs 3 and 15b; Altner, 1991). (c) By the early Late Cretaceous, when the subduction zone jumped inboard, most of the Tethyan oceanic lithosphere was already subducted, and minor accretion took place during the Late Cretaceous (Fig. 15d).

## 10. Conclusions

1. The ophiolitic mélangé in the Beynam (Ankara) region consists of distinct subduction-accretion units distinguished by lithology, age, structure and geochemistry, which were tectonically assembled mainly during the Late Jurassic and Early Cretaceous oceanic subduction.
2. In the Beynam (Ankara) region three subduction-accretion units (AU) are defined (Fig. 4). The structurally lowest one is a serpentinite mélangé; the intermediate one, the Otlubel AU, is a semi-intact Late Jurassic oceanic crust with a boninite geochemistry; and the topmost Holos AU consists of OIB-type alkali basalts with Upper Triassic seamount-derived shallow marine limestones and Middle to Upper Jurassic radiolarian cherts and pelagic limestones.
3. The Late Jurassic oceanic crust was formed above a subduction zone, and then was incorporated into an accretionary complex, when the subduction jumped inboard in the early



- Late Cretaceous creating an Andean-type convergent margin (Fig. 15).
- The ophiolitic mélange is stratigraphically overlain by a fore-arc turbidite sequence (the Haymana Formation), the base of which is dated to early to middle Campanian (c. 81 Ma). This provides an upper age limit for the tectonic assembly of the ophiolitic mélange in the Beynam area. The detrital zircons from basal sandstones in the fore-arc sequence are dominated by Santonian and Campanian zircons (87–81 Ma) derived from the magmatic arc.
  - Unlike most other subduction-accretion complexes, the ophiolitic mélange consists solely of oceanic crustal units and is devoid of land-derived coarse-clastic rocks. This is due to accretion occurring in an intra-oceanic subduction zone away from continental influence. During the Late Jurassic and Early Cretaceous period, the upper plate, the Sakarya Zone, was also a site of marine carbonate deposition (Fig. 3) and hence was not a source of clastic sediment.
  - During the Late Cretaceous the ophiolitic mélange, the fore-arc sequence (the Haymana Formation) and the Palaeo-Galatian arc formed a N–S-trending Andean-type convergent margin.
  - Ophiolitic mélanges are generally defined as monolithic units; however, geological mapping in the Beynam area has shown that at least locally they can be divided into distinct mappable tectonic units defined by lithology, age and geochemistry.
  - Ophiolitic mélanges in Anatolia are generally considered as of Late Cretaceous age; however, data from the Ankara region show that they formed mostly during the Late Jurassic and Early Cretaceous.

**Supplementary material.** To view supplementary material for this article, please visit <https://doi.org/10.1017/S0016756822000504>

**Acknowledgements.** This study was supported by İTÜ-BAP project (AIO and EÖ, project no. 41644) and by TÜBA for AIO. T.D. thanks the Région Hauts-de-France, the Ministère de l'Enseignement Supérieur et de la Recherche (CPER Climibio) and the European Fund for Regional Economic Development for their financial support. We thank Bora Rojay for discussions on the geology of the Ankara region. Ezgi Sağlam, Sinan Yılmaz and Turgut Duzman are thanked for help with rock preparation and mineral separation and Ali Osman Yücel and Sylvie Régnier for help with palaeontological preparations. We also thank Alastair Robertson and an anonymous reviewer for detailed and constructive reviews, which improved the text.

## References

- Akdoğan R, Okay AI and Dunkl I** (2018) Triassic–Jurassic arc magmatism in the Pontides as revealed by the U–Pb detrital zircon ages in the Jurassic sandstones, northeastern Turkey. *Turkish Journal of Earth Sciences* **27**, 89–109.
- Akdoğan R, Okay AI and Dunkl I** (2019) Striking variation in the provenance of the Lower and Upper Cretaceous turbidites in the central Pontides (northern Turkey) related to the opening of the Black Sea. *Tectonics* **38**, 1050–69.
- Akyürek B, Duru M, Sütçü YF, Papak İ, Şaroğlu F, Pehlivan N, Gönenç O, Granit S and Yaşar T** (1997) *Geological Map of Turkey – Ankara F15 (I29) Sheet and Explanatory Text. Scale 1:100 000*. Ankara: Maden Tetkik ve Arama Genel Müdürlüğü, 1 sheet, 31 pp. (in Turkish).
- Al-Shaibani SK, Carter DJ and Zaninetti L** (1983) Geological and micro-paleontological investigations in the Upper Triassic (Asinepe Limestone) of Seram, Outer Banda Arc, Indonesia. *Archives des Sciences, Genève* **36**, 297–313.
- Altner D** (1991) Microfossil biostratigraphy (mainly foraminifers) of the Jurassic–Lower Cretaceous carbonate successions in North-Western Anatolia (Turkey). *Geologica Romana* **27**, 167–213.
- Altner D, Koçyiğit A, Farinacci A, Nicosia U and Conti MA** (1991) Jurassic–Lower Cretaceous stratigraphy and paleogeographic evolution of the southern part of North-Western Anatolia. *Geologica Romana* **27**, 13–80.
- Altner D and Özkan S** (1991) Calpionellid zonation in North-Western Anatolia (Turkey) and calibration of the stratigraphic ranges of some benthic foraminifera at the Jurassic–Cretaceous boundary. *Geologica Romana* **27**, 215–35.
- Altner D and Zaninetti L** (1980) Le Trias dans la région de Pinarbasi, Taurus oriental, Turquie: unités lithologique, micropaléontologie, milieu de dépôt. *Rivista Italiana di Paleontologia* **86**, 705–60.
- Bailey EB and McCallien WJ** (1950) The Ankara Melange and the Anatolian Thrust. *Nature* **166**, 938–40.
- Bailey EB and McCallien WJ** (1953) Serpentinite lavas, the Ankara mélange and the Anatolian thrust. *Transactions of the Royal Society of Edinburgh* **62**, 403–42.
- Balci U and Sayit K** (2020) Diabase dykes from Boğazkale (Çorum), Central Anatolia: geochemical insights into the geodynamical evolution of the northern branch of Neotethys. *Geochemistry* **80**, 125602.
- Baumgartner O, Bartolini A, Carter E, Conti M, Cortese G, Danelian T, De Wever P, Dumitrica P, Dumitrica-Jud R, Gorican S, Guex J, Hull DM, Kito N, Marcucci M, Matsuoka A, Murchey B, O'Dogherty L, Savary J, Vishnevskaya V, Widz, D and Yao A** (1995) Middle Jurassic to Early Cretaceous radiolarian biochronology of Tethys based on Unitary Associations, In *Middle Jurassic to Lower Cretaceous Radiolaria of Tethys: Occurrences, Systematics, Biochronology* (eds O Baumgartner, L O'Dogherty, S Gorican, E Urquhart, A Pilleveit and P de Wever), pp. 1013–48. Mémoire de Géologie (Lausanne) no. 23.
- Bilgütay U** (1960) Geology of the Hasanöğlan-Ankara region. *Bulletin of Mineral Research and Exploration* **54**, 44–51.
- Bortolotti V, Chiari, M, Göncüoğlu MC, Principi G, Saccani E, Tekin UK and Tassinari R** (2018) The Jurassic–Early Cretaceous basalt–chert association in the ophiolites of the Ankara Mélange, east of Ankara, Turkey: age and geochemistry. *Geological Magazine* **155**, 451–78.
- Bortolotti V, Chiari M, Göncüoğlu MC, Marcucci M, Principi G, Tekin UK, Saccani E and Tassinari R** (2013) Age and geochemistry of basalt–chert associations in the ophiolites of the Izmir-Ankara mélange east of Ankara, Turkey: preliminary data. *Ophioliti* **38**, 157–73.
- Boynton WV** (1984) Geochemistry of Rare Earth Elements: Meteorite Studies, In *Rare Earth Element Geochemistry* (ed. P Henderson), pp. 63–114. New York: Elsevier.
- Bragin NY and Tekin UK** (1996) Age of radiolarian chert blocks from the Senonian ophiolitic mélange (Ankara, Turkey). *The Island Arc* **5**, 114–22.
- Burg J-P** (2018) Geology of the onshore Makran accretionary wedge: synthesis and tectonic interpretation. *Earth-Science Reviews* **185**, 1210–31.
- Çapan U and Floyd A** (1989) Geochemical and petrographic features of metabasalts within units of the Ankara Melange, Turkey. *Ophioliti* **10**, 3–18.
- Çapan UZ and Buket E** (1975) Geology of Aktepe–Gökdere Region and ophiolitic mélange. *Türkiye Jeoloji Kurumu Bülteni* **18**, 11–6 (in Turkish).
- Çelik Ö, Chiaradia M, Marzoli A, Billor Z and Marschik R** (2013) The Eldivan ophiolite and volcanic rocks in the İzmir–Ankara–Erzincan suture zone, Northern Turkey: geochemistry, whole-rock geochemical and Nd–Sr–Pb isotopic characteristics. *Lithos* **172–173**, 31–46.
- Çelik Ö, Marzoli A, Marschik R, Chiaradia M, Neubauer F and Öz İ** (2011) Early–Middle Jurassic intra-oceanic subduction in the İzmir–Ankara–Erzincan Ocean, Northern Turkey. *Tectonophysics* **509**, 120–34.
- Çelik ÖF, Özkan M, Chelle-Michou C, Sherlock S, Marzoli A, Ulianov A, Altıntaş İE and Topuz G** (2018) Blueschist facies overprint of late Triassic Tethyan oceanic crust in a subduction–accretion complex in north-central Anatolia, Turkey. *Journal of the Geological Society, London* **176**, 945–57.
- Çetin H, Demirel IH and Gökçen SL** (1986) Sedimentological and petrological study of the Upper Cretaceous – Lower Tertiary sequence east and west of Haymana (SW Ankara). *Türkiye Jeoloji Kurumu Bülteni* **29**, 21–33 (in Turkish).
- Chablais J, Martini R, Samankassou E, Onoue T and Sano H** (2010) Microfacies and depositional setting of the Upper Triassic midoceanic

- atoll-type carbonates of the Sambosan Accretionary Complex (southern Kyushu, Japan). *Facies* **56**, 249–78.
- Coleman RG and Peterman ZE** (1975) Oceanic plagiogranite. *Journal of Geophysical Research* **80**, 1099–108.
- Crawford AJ and Cameron WE** (1985) Petrology and geochemistry of Cambrian boninites and low-Ti andesites from Heathcote, Victoria. *Contributions to Mineralogy and Petrology* **91**, 93–104.
- Crawford AJ, Falloon TJ and Green DH** (1989) Classification petrogenesis and tectonic setting of boninites. In *Boninites and Related Rocks* (ed. AJ Crawford), pp. 1–49. London: Unwin Hyman.
- Danelian T, Asatryan G, Galoyan GH, Sahakyan L and Stepanyan J** (2016) Late Jurassic – Early Cretaceous radiolarian age constraints from the sedimentary cover of the Amasia ophiolite (NW Armenia), at the junction between the Izmir-Ankara-Erzincan and Sevan-Hakari suture zones. *International Journal of Earth Sciences* **150**, 67–80.
- Danelian T, Asatryan G, Sahakyan L, Galoyan GH, Sosson M and Avagyan A** (2010) New and revised Radiolarian biochronology for the sedimentary cover of ophiolites in the Lesser Caucasus (Armenia). In *Sedimentary Basin Tectonics from the Black Sea and Caucasus to the Arabian Platform* (eds M Sosson, N Kaymakci, RA Stephenson, F Bergerat and V Starostenko), pp. 383–91, Geological Society of London, Special Publication no. 340.
- Dangerfield A, Harris R, Sarifakioglu E and Dilek Y** (2011) Tectonic evolution of the Ankara Mélange and associated Eldivan ophiolite near Hançılı, Central Turkey. *Geological Society of America Special Paper* **480**, 143–69.
- Dilek Y and Ogawa Y** (2021) Subduction zone processes and crustal growth mechanisms at Pacific Rim convergent margins: modern and ancient analogues. *Geological Magazine* **158**, 1–12.
- Dilek Y and Thy P** (2006) Age and petrogenesis of plagiogranite intrusion in the Ankara mélange, central Turkey. *Island Arc* **15**, 44–57.
- Dönmez M, Akçay AE, Kara H, Yergök AF and Esentürk K** (2008) *Geological Map of Turkey – Kırşehir 130 Sheet and Explanatory Text. Scale 1:100 000*. Ankara: Maden Tetkik ve Arama Genel Müdürlüğü, 1 sheet, 26 pp. (in Turkish).
- Ernst WG** (2011) Accretion of the Franciscan Complex attending Jurassic–Cretaceous geotectonic development of northern and central California. *Geological Society of America Bulletin* **123**, 1667–78.
- Festa A, Ogata K and Pini GA** (2020) Polygenetic mélanges: a glimpse on tectonic sedimentary and diapiric recycling in convergent margins. *Journal of the Geological Society, London* **177**, 551–61.
- Floyd A** (1993) Geochemical discrimination and petrogenesis of alkalic basalt sequences in part of the Ankara mélange, central Turkey. *Journal of the Geological Society, London* **150**, 541–50.
- Gökten E and Floyd A** (2007) Stratigraphy and geochemistry of pillow basalts within the ophiolitic mélange of the Izmir-Ankara-Erzincan suture zone: implications for the geotectonic character of the northern branch of Neotethys. *International Journal of Earth Sciences* **96**, 725–41.
- Göncüoğlu MC, Sayit K and Tekin UK** (2010) Oceanization of the northern Neotethys: geochemical evidence from ophiolitic mélange basalts within the Izmir-Ankara suture belt, NW Turkey. *Lithos* **116**, 175–87.
- Göncüoğlu MC, Yalınz MK and Tekin UK** (2006) Geochemistry tectono-magmatic discrimination and radiolarian ages of basic extrusives within the İzmir-Ankara suture belt (NW Turkey): time constraints for the Neotethyan evolution. *Ofioliti* **31**, 25–38.
- Görür N, Oktay FY, Seymen İ and Şengör AMC** (1984) Paleotectonic evolution of the Tuzgölü basin complex Central Anatolia: sedimentary record of a Neo-Tethyan closure. In *The Geological Evolution of the Eastern Mediterranean* (eds JE Dixon and AHF Robertson), pp. 455–66. Geological Society of London, Special Publication no. 17.
- Gülyüz E, Kaymakci N, Meijers MJM, van Hinsbergen DJJ, Lefebvre C, Vissers RLM, Bart WH, Hendriks BWH and Peynircioglu AA** (2013) Late Eocene evolution of the Çiçekdağı Basin (central Turkey): syn-sedimentary compression during microcontinent-continent collision in central Anatolia. *Tectonophysics* **602**, 286–99.
- Gülyüz E, Özkaptan M, Kaymakci N, Persano C and Stuart FM** (2019) Kinematic and thermal evolution of the Haymana Basin, a fore-arc to fore-land basin in Central Anatolia (Turkey). *Tectonophysics* **766**, 326–39.
- Isozaki Y** (1997) Jurassic accretion tectonics of Japan. *The Island Arc* **6**, 25–51.
- Isozaki Y, Maruyama S and Furuoka F** (1990) Accreted oceanic materials in Japan. *Tectonophysics* **181**, 179–205.
- Kaymakci N, Özçelik Y, White SH and van Dijk M** (2009) Tectono-stratigraphy of the Çankırı Basin: Late Cretaceous to early Miocene evolution of the Neotethyan Suture Zone in Turkey. In *Collision and Collapse at the Africa–Arabia–Eurasia Subduction Zone* (eds DJJ van Hinsbergen, MA Edwards and R Govers), pp. 67–106. Geological Society of London, Special Publication no. 311.
- Koçyiğit A** (1989) The tectono-stratigraphy of the Hasanoğlan (Ankara) region: the evolution of the Karakaya orogenic belt. *Yerbilimleri* **14**, 269–94 (in Turkish).
- Koçyiğit A** (1991) An example of an accretionary forearc basin from northern Central Anatolia and its implications for the history of subduction of Neo-Tethys in Turkey. *Geological Society of America Bulletin* **103**, 22–36.
- Koçyiğit A, Winchester JA, Bozkurt E and Holland G** (2003) Saraçköy volcanic suite: implications for the subductional phase of arc evolution in the Galatian arc complex, Ankara, Turkey. *Geological Journal* **38**, 1–14.
- Kusky TM, Windley BF, Safonova I, Wakita K, Wakabayashi J, Polat A and Santosh M** (2013) Recognition of ocean plate stratigraphy in accretionary orogens through Earth history: a record of 3.8 billion years of sea floor spreading subduction and accretion. *Gondwana Research* **24**, 501–47.
- Kylander-Clark ARC, Hacker BR and Cottle JM** (2013) Laser-ablation split-stream ICP petrochronology. *Chemical Geology* **345**, 99–112.
- Lefebvre C, Barnhoorn A, van Hinsbergen DJJ, Kaymakci N and Vissers RLM** (2011) Late Cretaceous extensional denudation along a marble detachment fault zone in the Kırşehir massif near Kaman, central Turkey. *Journal of Structural Geology* **33**, 1220–36.
- Lefebvre C, Meijers MJM, Kaymakci N, Peynircioglu A, Langereis CG and van Hinsbergen DJJ** (2013) Reconstructing the geometry of Central Anatolia during the late Cretaceous: large-scale Cenozoic rotations and deformation between the Pontides and Taurides. *Earth and Planetary Science Letters* **366**, 83–98.
- Maffione M, van Hinsbergen DJJ, de Gelder GINO, van der Goes FC and Morris A** (2017) Kinematics of Late Cretaceous subduction initiation in the Neo-Tethys Ocean reconstructed from ophiolites of Turkey, Cyprus and Syria. *Journal of Geophysical Research: Solid Earth* **122**, 3953–76.
- Martini R, Peybernes B and Moix P** (2009) Late Triassic foraminifera in reefal limestones of SW Cyprus. *Journal of Foraminiferal Research* **39**, 218–30.
- Martini R, Zaninetti L, Lathuillière B, Cirilli S, Cornée J-J and Villeneuve M** (2004) Upper Triassic carbonate deposits of Seram (Indonesia): palaeogeographic and geodynamic implications. *Palaeogeography Palaeoclimatology Palaeoecology* **206**, 75–102.
- McCall GJH and Kidd RGW** (1982) The Makran, southeastern Iran: the anatomy of a convergent margin active from Cretaceous to present. In *Trench Forearc Geology: Sedimentation and Tectonics of Modern and Ancient Plate Margins* (ed JK Leggett), pp. 387–97. Geological Society of London, Special Publication no. 10.
- McDonough WF and Sun SS** (1995) The composition of the Earth. *Chemical Geology* **120**, 223–53.
- Meijers MJM, Kaymakci N, van Hinsbergen DJJ, Langereis CG, Stephenson RA and Hippolyte J-C** (2010) Late Cretaceous to Paleocene oroclinal bending in the central Pontides (Turkey). *Tectonics* **29**, TC4016.
- Mueller MA, Licht A, Campbell C, Oçaklıoğlu F, Taylor MH, Burch L, Ugrai T, Kaya M, Kurtoğlu B, Coster MC, Métails G and Beard KC** (2019) Collision chronology along the İzmir-Ankara-Erzincan suture zone: insights from the Sarıcakaya Basin western Anatolia. *Tectonics* **38**, 3652–74.
- Nairn SP, Robertson AHF, Ünlügenç UC, Taslı K and Inan N** (2013) Tectonostratigraphic evolution of the Upper Cretaceous–Cenozoic central Anatolian basins: an integrated study of diachronous ocean basin closure and continental collision. In *Geological Development of Anatolia and the Easternmost Mediterranean Region* (eds AHF Robertson, O Parlak and UC Ünlügenç), pp. 343–84. Geological Society of London, Special Publication no. 372.
- Norman TN** (1972) Stratigraphy of the Upper Cretaceous–Lower Tertiary strata of Ankara Yahşıhan area. *Türkiye Jeoloji Kurumu Bülteni* **15**, 180–276 (in Turkish).
- Nunn D, Kumar L, Eliot I and McLean RF** (2016) Classifying Pacific islands. *Geoscience Letters* **3**, 7. doi: [10.1017/S0016756822000504](https://doi.org/10.1017/S0016756822000504)



- Okay AI and Altuner D** (2016) Carbonate sedimentation in an active margin: Cretaceous history of the Haymana region Pontides. *International Journal of Earth Sciences* **105**, 2013–30.
- Okay AI, Altuner D and Kylander-Clark ARC** (2019) Major Late Cretaceous mass flows in central Turkey recording the disruption of the Mesozoic continental margin. *Tectonics* **38**, 960–89.
- Okay AI, Harris NBW and Kelley SP** (1998) Exhumation of blueschists along a Tethyan suture in northwest Turkey. *Tectonophysics* **285**, 275–99.
- Okay AI and Nikishin AM** (2015) Tectonic evolution of the southern margin of Laurasia in the Black Sea region. *International Geology Review* **57**, 1051–76.
- Okay AI, Sunal G, Sherlock S, Kylander-Clark ARC and Özcan E** (2020a) İzmir-Ankara suture as a Triassic to Cretaceous plate boundary: data from central Anatolia. *Tectonics* **38**, e2019TC005849.
- Okay AI and Tüysüz O** (1999) Tethyan sutures of northern Turkey. In *The Mediterranean Basins: Tertiary Extension within the Alpine Orogen* (eds B Durand, L Jolivet, F Horváth and M Séranne), pp. 475–515. Geological Society of London, Special Publication no. 156.
- Okay AI, Zattin M, Özcan E and Sunal G** (2020b) Uplift of Anatolia. *Turkish Journal of Earth Sciences* **29**, 696–713.
- Özkan M, Çelik ÖF, Soycan H, Çörtük RM and Marzoli A** (2020) The Middle Jurassic and Early Cretaceous basalt-radiolarian chert association from the Tekelidağ Mélange eastern İzmir-Ankara-Erzincan suture zone (northern Turkey). *Cretaceous Research* **107**, 104280.
- Öztürk YY, Helvacı C and Satır M** (2012) Geochemical and isotopic constraints on petrogenesis of the Beypazarı Granitoid, NWAnkara, western central Anatolia, Turkey. *Turkish Journal of Earth Sciences* **21**, 53–77.
- Pandeli E, Elter FM, Toksoy-Köksal F, Principi G, Orlando A, Valleri G, Giusti R and Orti L** (2018) Relationships between the Sakarya Zone and the Ankara-Erzincan suture (central-northern Turkey): geological and petrographic data from the Ankara-Çankiri Çorum and Amasya areas. *Geological Magazine* **155**, 506–35.
- Parlak O and Robertson, AHF** (2004) The ophiolite-related Mersin Melange, southern Turkey: its role in the tectonic-sedimentary setting of Tethys in the Eastern Mediterranean region. *Geological Magazine* **141**, 257–86.
- Paterson SR and Ducea MN** (2015) Arc magmatic tempos: gathering the evidence. *Elements* **11**, 91–8.
- Pearce JA** (1996) A user's guide to basalt discrimination diagrams. In *Trace Element Geochemistry of Volcanic Rocks: Applications for Massive Sulphide Exploration* (ed. DA Wyman), pp. 79–113. Geological Association of Canada, Geochemistry Short Course Notes no. 12.
- Pearce JA** (2008) Geochemical fingerprinting of oceanic basalts with applications to ophiolite classification and the search for Archean oceanic crust. *Lithos* **100**, 14–48.
- Pearce JA and Reagan MK** (2019) Identification, classification and interpretation of boninites from Anthropocene to Eoarchean using Si-Mg-Ti systematics. *Geosphere* **15**, 1008–37.
- Pearce JA, van der Laan SR, Arculus RJ, Murton BJ, Ishii T, Peate DW and Parkinson I** (1992) Boninite and harzburgite from Leg 125 (Bonin-Mariana forearc): a case study of magma genesis during the initial stages of subduction. In *Proceedings of the Ocean Drilling Program, Scientific Results, vol. 125* (eds P Fryer, JA Pearce, LB Stokking *et al.*), pp. 623–59. College Station, Texas
- Plunder A, Agard P, Chopin C and Okay AI** (2013) Geodynamics of the Tavşanlı zone, western Turkey: insights into subduction/obduction processes. *Tectonophysics* **608**, 884–903.
- Premoli Silva I and Verga D** (2004) Practical manual of Cretaceous planktonic foraminifera. In *International School on Planktonic Foraminifera 3° Course: Cretaceous* (eds D Verga and R Rettori), pp. 1–283. Tipografia Pontefelcino Perugia (Italy): Universities of Perugia and Milan.
- Raymond LA** (1984) Classification of mélanges. In *Mélanges: Their Nature, Origin and Significance* (ed. LA Raymond), pp. 7–20. Geological Society of America, Special Paper no. 198.
- Raymond LA** (2018) What is Franciscan?: revisited. *International Geology Review* **60**, 1968–2030.
- Raymond LA, Ogawa Y and Maddock ME** (2020) Accretionary unit formats in subduction complexes: examples from the Franciscan and Miura-Boso complexes. *International Geology Review* **62**, 1581–609.
- Robertson, AHF, Parlak O and Dumitrica P** (2021) Role of Late Cretaceous volcanic-sedimentary mélanges, specifically the Aladağ melange, E Turkey, in the rift-drift-subduction-accretion-emplacment history of the Tethyan Inner Tauride ocean. *International Geology Review*. doi: [10.1080/00206814.2021.1925980](https://doi.org/10.1080/00206814.2021.1925980).
- Robertson, AHF, Parlak O, Ustaömer T, Taşlı K, İnan N, Dumitrica P and Karaoğlan F** (2013) Subduction, ophiolite genesis and collision history of Tethys adjacent to the Eurasian continental margin: new evidence from the Eastern Pontides, Turkey. *Geodinamica Acta* **26**, 230–93.
- Robertson AHF, Parlak O and Ustaömer T** (2009) Melange genesis and ophiolite emplacement related to subduction of the northern margin of the Tauride-Anatolide continent, central and western Turkey. In *Collision and Collapse at the Africa-Arabia-Eurasia Subduction Zone* (eds DJJ van Hinsbergen, MA Edwards and R Govers), pp. 9–66. Geological Society of London, Special Publication no. 311.
- Robertson AHF and Ustaömer T** (2012) Testing alternative tectono-stratigraphic interpretations of the Late Palaeozoic Early Mesozoic Karakaya Complex in NW Turkey: support for an accretionary origin related to northward subduction of Palaeotethys. *Turkish Journal of Earth Sciences* **21**, 961–1007.
- Rojay B** (2013) Tectonic evolution of the Cretaceous Ankara Ophiolitic Mélange during the Late Cretaceous to pre-Miocene interval in Central Anatolia Turkey. *Journal of Geodynamics* **65**, 66–81.
- Rojay B, Altuner D, Özkan-Altuner S, Önen AP, James S and Thirlwall MF** (2004) Geodynamic significance of the Cretaceous pillow basalts from North Anatolian Ophiolitic Melange Belt (Central Anatolia, Turkey): geochemical and paleontological constraints. *Geodinamica Acta* **17**, 349–61.
- Rojay B, Yalınız K and Altuner D** (2001) Age and origin of some pillow basalts from Ankara mélange and their tectonic implications to the evolution of northern branch of Neotethys Central Anatolia. *Turkish Journal of Earth Sciences* **10**, 93–102.
- Rolland Y, Galoyan G, Sosson M, Melkonyan R and Avagyan A** (2010) The Armenian Ophiolite: insights for Jurassic back-arc formation, Lower Cretaceous hot spot magmatism, and Upper Cretaceous obduction over the South Armenian Block. In *Sedimentary Basin Tectonics from the Black Sea and Caucasus to the Arabian Platform* (eds M Sosson, N Kaymakci, RA Stephenson, F Bergerat and V Starostenko), pp. 353–82. Geological Society of London, Special Publication no. 340.
- Sano S and Kanmera K** (1991) Collapse of ancient oceanic reef complex – What happened during collision of Akiyoshi reef complex? – Limestone breccia redeposited limestone debris and mudstone injection. *Journal of the Geological Society of Japan* **97**, 297–309.
- Sarıfakıoğlu E, Dilek Y and Sevin M** (2014) Jurassic-Paleogene intraoceanic magmatic evolution of the Ankara Mélange, north-central Anatolia, Turkey. *Solid Earth* **5**, 77–108.
- Sarıfakıoğlu E, Dilek Y and Sevin M** (2017) New synthesis of the İzmir-Ankara-Erzincan suture zone and the Ankara mélange in northern Anatolia based on new geochemical and geochronological constraints. *Geological Society of America Special Paper* **525**, 1–62.
- Şenel M** (2002) *Geological Map of Turkey – Kayseri Sheet. Scale 1:500 000*. Ankara: Maden Tetkik ve Arama Genel Müdürlüğü Ankara, 1 sheet.
- Şengör AMC and Yılmaz Y** (1981) Tethyan evolution of Turkey: a plate tectonic approach. *Tectonophysics* **75**, 181–241.
- Senowbari-Daryan B and Link M** (2017) Foraminifera from the Norian-Rhaetian reef carbonates of the Taurus Mountains (Saklıkent Turkey). *Geologica Carpathica* **68**, 303–17.
- Sharman GR, Graham SA, Grove M, Kimbrough DL and Wright JE** (2015) Detrital zircon provenance of the Late Cretaceous-Eocene California forearc: influence of Laramide low-angle subduction on sediment dispersal and paleogeography. *Geological Society of America Bulletin* **127**, 38–60.
- Stern R J** (2002) Subduction zones. *Reviews of Geophysics* **40**, 1012.
- Sun SS and McDonough WF** (1989) Chemical and isotopic systematics of oceanic basalts: implications for mantle composition and processes. In *Magmatism in the Ocean Basins* (eds AD Saunders and MJ Norry), pp. 313–45. Geological Society of London, Special Publication no. 42.
- Taira A, Katto J, Tashiro M, Okamura M and Kodama K** (1988) The Shimanto Belt in Shikoku Japan: evolution of Cretaceous to Miocene accretionary prism. *Modern Geology* **12**, 5–46.

- Tankut A, Dilek Y and Önen P** (1998) Petrology and geochemistry of the Neotethyan volcanism as revealed in the Ankara Melange Turkey. *Journal of Volcanology and Geothermal Research* **85**, 265–84.
- Tekin UK, Göncüoğlu MC and Turhan N** (2002) First evidence of Late Carnian radiolarian fauna from the Izmir-Ankara Suture Complex, Central Sakarya, Turkey: implications for the opening age of the Izmir-Ankara branch of Neotethys. *Geobios* **35**, 127–35.
- Topuz G, Çelik ÖF, Şengör AMC, Altıntaş İE, Zack T, Rolland Y and Barth M** (2013) Jurassic ophiolite formation and emplacement as backstop to a subduction-accretion complex in Northeast Turkey: the Refahiye ophiolite and relation to the Balkan ophiolites. *American Journal of Science* **313**, 1054–87.
- Topuz G, Okay AI, Altherr R, Meyer H-P and Nasdala L** (2006) Partial high-pressure aragonitization of micritic limestones in an accretionary complex, Tavşanlı Zone, NW Turkey. *Journal of Metamorphic Geology* **24**, 603–13.
- Turhan N** (2002) *Geological Map of Turkey – Ankara Sheet. Scale 1:500 000*. Ankara: Maden Tetkik ve Arama Genel Müdürlüğü, 1 sheet.
- Ünal G** (1981) The stratigraphy of the “Ankara Melange” southwest of Ankara. In *Proceedings of the Symposium on the Geology of the Central Anatolia*, pp. 46–52. Ankara: Türkiye Jeoloji Kurumu (in Turkish).
- Ünal G, Yüksel V, Tekeli T, Gönenç O, Seyirt Z and Hüseyin S** (1976) Upper Cretaceous–Lower Tertiary stratigraphy and paleogeographic evolution of the Haymana–Polatlı region (southwest Ankara). *Türkiye Jeoloji Kurumu Bülteni* **19**, 159–76 (in Turkish).
- Uysal I, Ersoy EY, Dilek Y, Escayola M, Sarifakioğlu E, Saka S and Hirata T** (2013) Depletion and refertilization of the Tethyan oceanic upper mantle as revealed by the early Jurassic Refahiye ophiolite, NE Anatolia-Turkey. *Gondwana Research* **27**, 594–611.
- van Hinsbergen DJJ, Maffione M, Plunder A, Kaymakçı N, Ganerod M, Hendriks BWH, Corfu F, Güler D, de Gelder GINO, Peters K, McPhee J, Brouwer FM, Advokaat EL and Vissers RLM** (2016) Tectonic evolution and paleogeography of the Kırşehir Block and the Central Anatolian Ophiolites, Turkey. *Tectonics* **35**, 983–1014.
- van Hinsbergen DJJ, Torsvik TH, Schmid SM, Matenco LC, Maffione M, Vissers RLM, Güler D and Spakman W** (2020) Orogenic architecture of the Mediterranean region and kinematic reconstruction of its tectonic evolution since the Triassic. *Gondwana Research* **81**, 79–229.
- Varol E** (2013) The derivation of potassic and ultrapotassic alkaline volcanic rocks from an orogenic lithospheric mantle source: the case of the Kalecik district, Ankara, Central Anatolia Turkey. *Neues Jahrbuch der Mineralogie Abhandlungen* **191**, 55–73.
- Wakabayashi J** (2015) Anatomy of a subduction complex: architecture of the Franciscan complex, California, at multiple length and time scales. *International Geology Review* **57**, 669–746.
- Wakita K and Metcalfe I** (2005) Ocean plate stratigraphy in East and Southeast Asia. *Journal of Asian Earth Sciences* **24**, 679–702.
- Whitney DL and Hamilton MA** (2004) Timing of high-grade metamorphism in central Turkey and the assembly of Anatolia. *Journal of the Geological Society* **161**, 823–8.
- Winchester JA and Floyd A** (1977) Geochemical discrimination of different magma series and their differentiation products using immobile elements. *Chemical Geology* **20**, 325–43.
- Zaninetti L** (1976) Les Foraminifères du Trias: Essai de synthèse et corrélation entre les domaines mésogéen européen et asiatique. *Rivista Italiana di Paleontologia* **82**, 1–258.
- Zaninetti L, Altner D, Dager Z and Ducret B** (1982) Les Milioliporidae (Foraminifères) dans le Trias supérieur à faciès récifal du Taurus Turquie. II. Microfaunes associées. *Revue de Paléobiologie* **1/2**, 105–39.